Pergamon

PII: S0079-6611(97)00009-8

*Prog. Oceanog.* Vol. 39, pp. 109–151, 1997

Printed in Great Britain
0079-6611/97 $32.00

# Evolution of satellite derived mesoscale thermal patterns in the Black Sea

HALİL İ. SUR[1] and YURI P. ILYIN[2]

[1]*Institute of Marine Sciences, Middle East Technical University, PK 28, Erdemli, İçel, 33731 Turkey*
[2]*Marine Hydrophysical Institute, Ukrainian Academy of Sciences, 2, Kapitanskaya Str., Sevastopol, 335000, Ukraine*

**Abstract** – Infrared image sequences covering the Black Sea are examined to investigate the evolution of mesoscale structures on the sea surface during the warm seasons of 1991–1993. Wind induced surface mixing and convective mixing are responsible for producing many features. The influence of seasonal evolution of the cold intermediate water (CIW) on the vertical and surface structures of eddies, including cold anticyclonic ones in summer, is examined. The annual variations of the short and long wave structures accompanying the meandering Rim Current are identified. The influence of river inputs to the western shelf area was traced more distinctly as evidence of the maximal outflow after the spring flood. Satellite data also helped in the interpretation of several peculiarities observed in vector distributions of the Acoustic Doppler Current Profiler (ADCP) observations resulting from sub-mesoscale dynamic features that were insufficiently resolved by the *in situ* data. The ADCP velocity maxima coincide with the temperature gradient of the Rim Current and the vector directions correspond to the satellite derived flow configuration in April 1993 implying a close correlation between both measurements. 

PROOCE 39-2-B

CONTENTS



## 1. INTRODUCTION

One of the fundamental problems in modern oceanography is the qualitative and quantitative description of interaction and exchange between the coastal (shelf) and deep regions of seas which is especially important for the utilization of ecological and marine resources. For an inland basin like the Black Sea (Fig. 1a), this problem is of primary significance.

The general circulation of the Black Sea consists of a basin scale cyclonic boundary current (so-called, Rim Current, OĞUZ *et al.*, 1993, 1994) with smaller scale circulations inshore of this main current, and also an intense anticyclonic gyre in the easternmost corner of the basin (Fig. 1b). Interconnecting series of cyclonic eddies and sub-basin scale gyres form the interior circulation. STANEV *et al.* (1988), LATUN (1990), and EREMEEV *et al.* (1991) all indicate that the circulation is more clearly defined and intense during winter than in summer; in summer, eddy activity is more pronounced at different scales which range from quasi-stationary gyres to small and shallow eddies. Some of these eddies are associated with the meandering Rim Current, while others are produced by atmospheric forcing and buoyancy fluxes either over a short-time period or on a seasonal basis. The strong Rim Current limits water and material transfer across the current zone while jet like instabilities, mesoscale eddies, filaments, mushroom-like structures and similar phenomena play important roles in cross-shelf (cross-frontal) shelf-deep water interactions. Spatial (10–100 km) and temporal (1–10 days) scales of these phenomena do not allow a full experimental description of their structures, generation and evolution based on traditional oceanographical measurements alone. Such study is only possible by co-analyses of hydrographic and satellite data.

Recent progress in satellite remote sensing of the infrared band (the most regular and accessible source of information) allows the resolution of problems posed by small- and mesoscale features in interpreting *in situ* observations. But very often, the use of such data alone lacks the full understanding of the formation of sea surface patterns under specific regional conditions. Thus, their analysis is limited by an inability to interpret surface structures which can sometimes leads to false conclusions because of water stratification and regional dynamic peculiarities. Development of physical methods for the joint use of satellite and ship data should be carried out in the regions where enough instrumental data are available. One such region is the Black Sea-inland basin with predictable oceanographic processes.

The aim of the present paper is to apply the methodologies for the analysis of satellite infrared

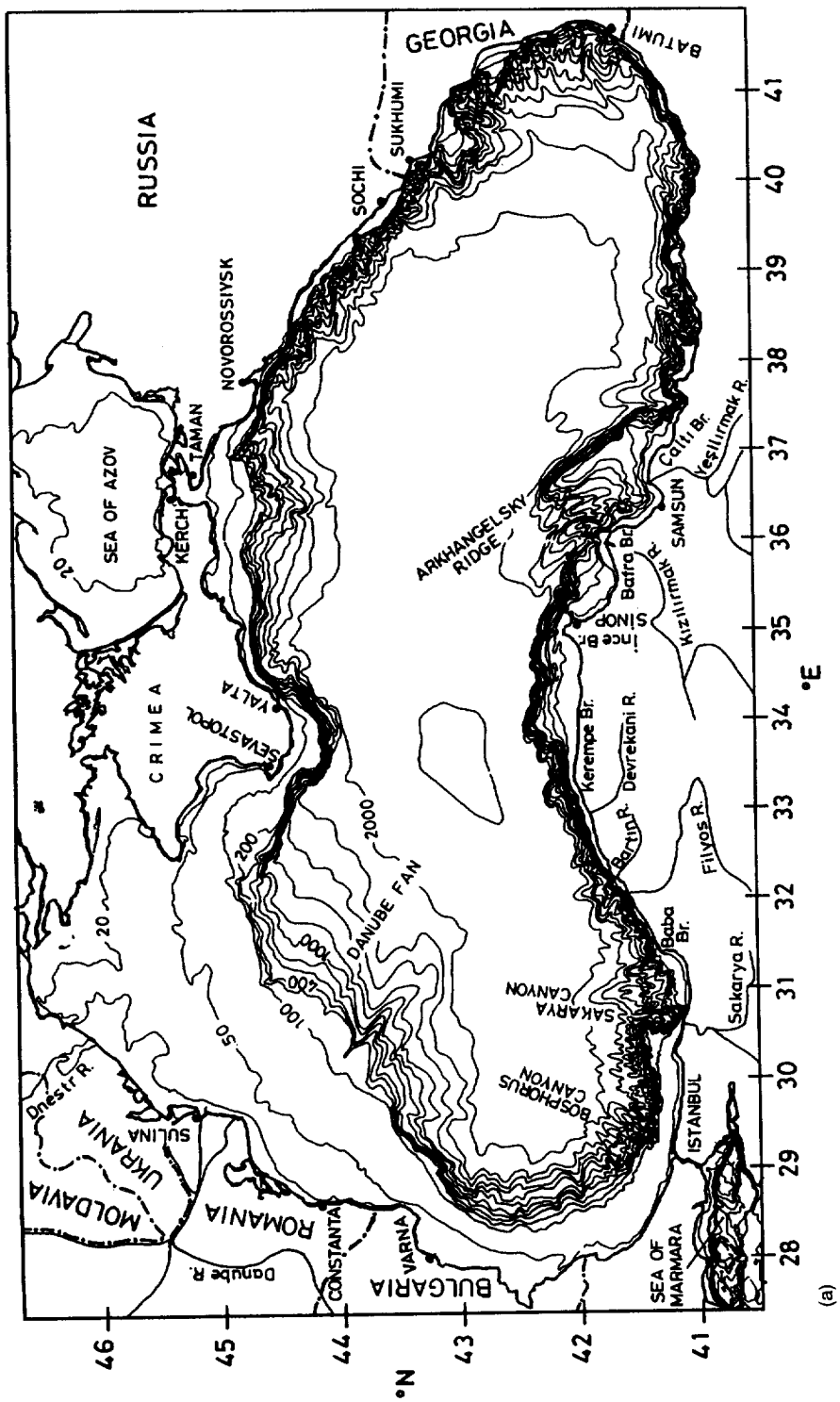


(a)

Fig. 1. (a) Bathymetry map of the Black Sea, (b) Schematised general circulation of the Black Sea.

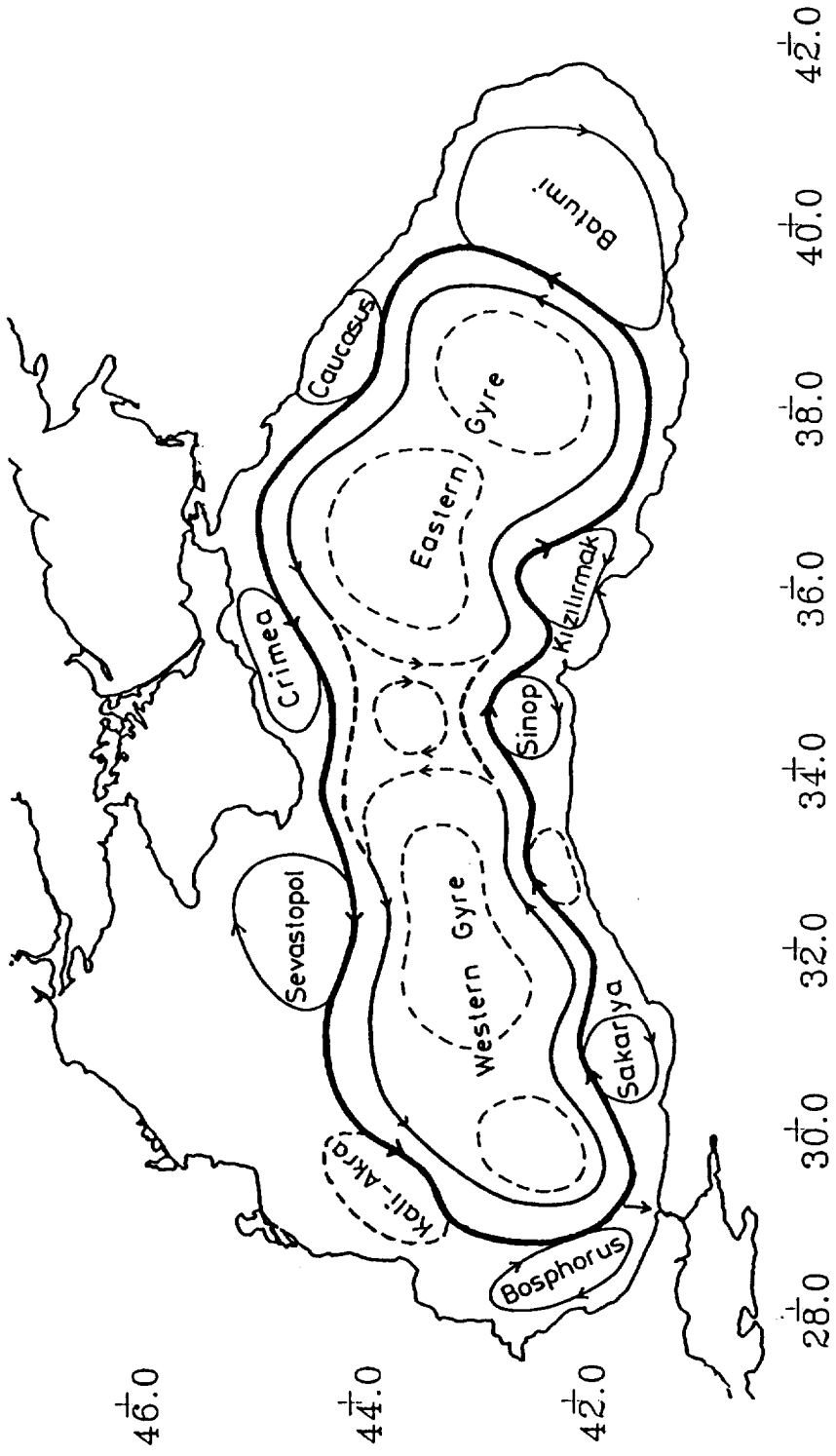


(b)

Fig. 1. Continued

imagery in describing mesoscale dynamics in relation to the formation mechanism of surface thermal patterns under specific Black Sea conditions, and to understand qualitatively and describe quantitatively regional dynamic features based on the methods developed earlier and the information collected in the framework of the CoMSBlack (Cooperative Marine Science Program for the Black Sea, ÜNLÜATA *et al.*, 1993) cruises. Attention is focussed on the dynamic processes driving the Shelf-Deep water interactions assuming that they are realized primarily by the influence of mesoscale processes.

GRISHIN *et al.* (1989a, b), ILYIN and GRISHIN (1992), IVANOV and ILYIN (1993), SUR *et al.* (1994, 1996) used a series of satellite images for description of qualitative and quantitative parameters of the large and mesoscale dynamical events. This work can be considered as a continuation and development of previous studies contributing to the international investigation of the Black Sea oceanography.

Data sets are described in Section 2. Section 3 concentrates on the physics of surface thermal patterns used to interpret the satellite images. The main part of the paper, Section 4, contains detailed analyses of satellite image sequences referring to selected regions of the Black Sea. Comparison between ADCP current measurements and satellite thermal patterns are discussed separately in Section 5. The concluding remarks are given in Section 6.

## 2. DATA AND METHODS

### *2.1. Ship measurements*

CTD-data, from the international cruises within the framework of the HydroBlack (September, 1991) and CoMSBlack (July, 1992 and April, 1993) programs, were used for establishing the hydrophysical properties of the Black Sea which were analyzed in the previous papers (OĞUZ *et al.*, 1993, 1994, 1996; and SUR *et al.*, 1994, 1996). Additional CTD-data sets were considered for the analysis of deep thermal structure in the Sevastopol anticyclonic region. These data sets were obtained during the hydrographic surveys undertaken by the Marine Hydrophysical Institute (MHI) west of Crimea in May, August and September of 1992 (IVANOV, 1992). ADCP current measurements on board the R/V *Bilim* were also performed both at hydrographic stations and along the ship tracks during the CoMSBlack-93 cruise. The data assembled were averaged over 10 minute intervals and then spatially averaged so that data points are separated by at least 5 km (GÜNGÖR, 1994). The distribution of horizontal current vectors at 10 m level (nearest to sea surface) were analyzed together with the satellite thermal images.

### *2.2. Satellite data*

Images obtained from NOAA-11 were used in the present work. This satellite has advanced multi-channel scanning radiometer AVHRR/2, and sends digital information in high resolution picture transmission mode (HRPT). AVHRR has five different bands; Channels 1 and 2 are in visible and near-infrared bands (600 and 900 nm), Channels 3, 4 and 5 are in thermal infrared windows (3.7, 10.8 and 11.8 $\mu$m). Software developed in MHI was used for the pre-processing, geographical positioning and geometrical transformation on to a rectangular projection map. The second stage of processing gives the surface distribution of digital radiation temperature for infrared channels. Their spatial resolution is 1′ along meridian and 1.5′ along parallel, and the radiation temperature resolution is about 0.1°C. Final analyses such as contrast enhancements,

coast and bathymetry overlapping were performed at the Institute of Marine Sciences – Middle East Technical University (IMS-METU). Forty cloud-free (or low-cloud) satellite images of Channel 4 were considered in the present paper. Atmospheric absorption in this part of spectrum is minimal, moreover, it is known that temperature differences for the distances on the order of 10–100 km can be estimated with an accuracy of about 0.1°C (within the sensitivity level of AVHRR/2)since the uniformity of local atmospheric conditions does not change too much on these scales. Night time images were preferred to eliminate the diurnal thermocline problem since the radiometric measurements of sea-surface (skin) temperature may differ significantly from the "bulk" sea-surface temperature (representative of top one or two metres) on sunny afternoons on relatively calm days (ROBINSON, 1991).

In this paper, our aim is not to investigate oceanographic parameter SST (bulk-temperature) distribution and its evolution, since a multichannel technique is not considered able to estimate the SST distribution from satellite images. Our goal is to interpret the surface manifestation of mesoscale processes in the radiational temperature field, to map their location, dimensions and configuration, as well as, to compare their characteristics with the results of traditional oceanographic studies.

The effects on skin-temperature and the diurnal thermocline is not discussed here, because these effects are strongly dependent on atmospheric conditions and have the same horizontal scales (much longer than mesoscale features of marine water circulation) (FEDOROV and GINSBURG, 1988). Intensive large-scale surface cooling and heating can smooth horizontal temperature gradients, so that the contrast of IR-images may sometimes be fairly weak. But, by using a time series of images, most of the dynamic patterns can be recognized. Therefore, in the next sections we assume that, the surface temperature is equivalent to upper mixed layer temperature, within an error of 0.1–0.3°C.

Separate regions of the Black Sea were considered during the analysis to examine the time evolution of the events more clearly. The white stars and line patterns on some of the images are where there is data dropout in the reception.

## 3. THERMAL MANIFESTATIONS OF MESOSCALE DYNAMICS ON THE SEA SURFACE

Three main mechanisms; advection, surface heating and turbulent entrainment influence the distribution of sea surface temperature (SST) in the Black Sea during the summer season; and a surface mixed layer with a very sharp seasonal thermocline at its base develops fully during the same season. The well-known equation for the evolution of temperature in the upper mixed layer can be written in the following form:

$$\partial T_s/\partial t = - V.\nabla T_s + (1/h)[Q_s/rC_p - (dh/dt)(T_s - T_h)] \quad (1)$$

where;

| | |
|---|---|
| $T_s$ | temperature of the mixed layer, which we suppose to be nearly equal to surface temperature, |
| $t$ | time, |
| $V$ | horizontal current vector, |
| $h$ | mixed layer depth, |
| $Q_s$ | net surface heat flux, |
| $C_p$ | specific heat at constant pressure, |
| $r$ | density of the sea water, |
| $T_h$ | water temperature just below the density (temperature) jump. |

The first term on the right hand side of Eq. (1) describes the advection of temperature by a current field. The second term inside the square brackets indicates the heat flux at the bottom of the mixed layer caused by turbulent entrainment of lower water up across the interface ($dh/dt$ is the entrainment speed).

When there are significant temperature gradients, the advection processes determining surface temperature features for the dynamically active regions and the evolution of SST isolines tend to follow the streamlines of surface circulation. This process results in S-like features and is an adjustment characteristic in the case of vortex fields (LINDEN, 1991). The amount of heat or cold advection is closely related to the orbital velocities of the eddies, and the thermal satellite images of these features generally have high contrasts.

During the summer season in the Black Sea, a sharp seasonal thermocline is formed by the influence of seasonal and diurnal heating. Surface heat flux, $Q_s$, depends mainly on atmospheric conditions, so that its spatial scale is much larger than that of mesoscale features in the sea; therefore, it tends to smooth the horizontal gradient in SST (i.e., $\nabla T_s$ decreases yielding to the weak mesoscale patterns). But sometimes under specific conditions, this mechanism can be important for the visualization of surface jets, eddies and fronts, as is seen in the case of seasonal thermocline formation or in shallow mixed layer regions. Parameters for the intense diurnal heating and mesoscale features can be evaluated by considering differences between day and night time satellite images of the same areas (ILYIN, 1989).

Entrainment of the cold subthermocline waters through the bottom boundary of the mixed layer results in more noticeable patterns at the sea surface, and this has been analyzed qualitatively in FEDOROV and GINSBURG (1988). Here, we consider its essence and give some simple quantitative estimates.

Assume that the previously formed upper mixed layer is separated from the underlying water by a sharp interface at depth $h_g$, and that its relief is related to the sea surface topography by $\delta h_g \approx (R/L)\delta\epsilon$ because of geostrophic adjustment; where $\delta h_g$, $\delta\epsilon$ are elevations of interface and surface respectively, $R$ - barotropic Rossby radius of deformation, $L$ - spatial scale of event (e.g., horizontal dimension of the eddy). Thus, for a typical sub-basin gyre in the Black Sea; $\delta h_g/\delta\epsilon \approx 100$, so that if the elevation of sea level is about 5–10 cm at the gyre center in comparison with its periphery, $\delta h_g$ would be $\approx$ 5–10 m.

It is known that the upper mixed layer depth tends to have an equilibrium state when the production of turbulent energy, which overcomes the buoyancy force, is balanced by its destruction (KRAUS *et al.*, 1988). The measure of this depth is the Obuchov's length which is defined as:

$$L_h = (rC_p u_*^3)/(\alpha g Q_s) \tag{2}$$

where;

$\alpha$ water thermal expansion coefficient,
$g$ gravitational acceleration,
$u_*$ dynamic velocity which is the function of wind speed.

It is clear from (2) that $L_h$ is determined by the atmospheric forcing, therefore, its variations are much less horizontally than vertically. To evaluate the characteristic value of $L_h$ for the Black Sea during the summer season, the following form of (2) can be used;

$$L_h = \beta W^3/Q_s \tag{3}$$

where;

| | |
|---|---|
| $\beta$ | $C_p(r_a C_d)^{1.5}/(\alpha g r^{0.5})$ |
| $W$ | wind speed, |
| $r_a$ | air density, |
| $C_d$ | drag coefficient, |
| $r$ | water density. |

Numerical value for $\beta$ is about 4.5 Joul.s$^2$.m$^{-4}$ for the Black Sea under summer conditions, and $Q_s$ is about 160 Joul.m$^{-2}$.s$^{-1}$ according to HANEY (1971). Assuming $0 \leq W \leq 10$ m.s$^{-1}$, then the calculated $L_h$ values are displayed in Fig. 2a. During the summer season, the expected value of $h_g$ is about 10–20 m, therefore, quite moderate wind speeds (7-9 m.s$^{-1}$) are enough for establishing the entrainment regime. At higher wind speeds, this mechanism leads to a smoothing of surface temperature as a result of total cooling in the upper mixed layer on the scales greater than L (e.g., horizontal dimension of eddy).

To estimate the value of the surface temperature anomaly produced by entrainment on the basis of Eq. (1), suppose that temperature and mixed layer depth change linearly from some initial values $T_0$ and $h_0$ to $T_s$ and $L_h$ respectively during the time interval $\delta$t (several hours or days). Thus, integration of the Eq. (1) yields:

$$(T_s - T_0) = Q_s \delta t / r C_p h_0 - [(L_h/h_0) - 1](T_0 - T_h) \tag{4}$$

where $L_h/h_0$ is the important parameter which drives anomalies resulting from entrainment, and can easily be evaluated by neglecting the effect of surface heating during the period of $\delta t$. Then Eq. (4) is expressed as;

$$(T_s - T_0) = (1 - L_h/h_0)(T_0 - T_h) \tag{5}$$

Considering $h_0 \leq L_h$ and $T_h \leq T_s \leq T_0$; expected anomalies in SST as a function of temperature difference between the upper and lower layers, and the parameter $L_h/h_0$ is plotted in Fig. 2b. When this ratio ($L_h/h_0$) is large, the turbulence is dominated by wind stirring; thermal convection becomes the dominant factor when the ratio is small and positive (NIILER and KRAUS, 1977).

Usually, shoaling of the interface ($h_g$) is associated with the centers of cyclonic eddies while its deepening is linked with the anticyclones. If $L_h$ is greater than $h_g = h_0$ at the center of the cyclone and does not exceed $h_g$ at its periphery, then the turbulent entrainment leads to an appearance of a cold anomaly and its magnitude is determined by the temperature difference ($T_0$–$T_s$). In anticyclones, we expect the opposite pattern, i.e., cold anomaly to occur around periphery of the eddy.

Peculiarities in the water structure of anticyclonic eddies on the right hand side of the Rim Current in the Black Sea produce deviations from the scheme described above. Typically, thickness of the CIW in these anticyclones significantly exceeds peripheral values in summer and the upper boundary of the CIW coincides with the lower boundary of the seasonal thermocline which is closer to the sea surface (BLATOV *et al.*, 1984); then turbulent entrainment leads to the appearance of cold anomalies over the center of anticyclonic eddies. By the end of the warm season, the volume of the CIW inside the anticyclones decreases and $h_g$ gets larger at their centers, therefore, we expect warm anomalies to occur at the centers of these anticyclones. Both of these situations are described schematically in Fig. 3.

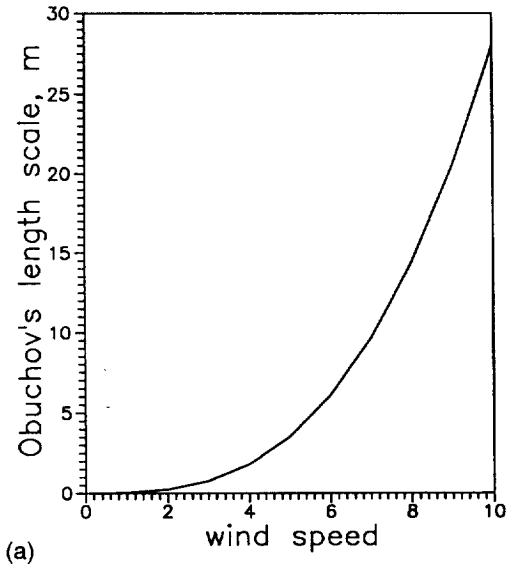


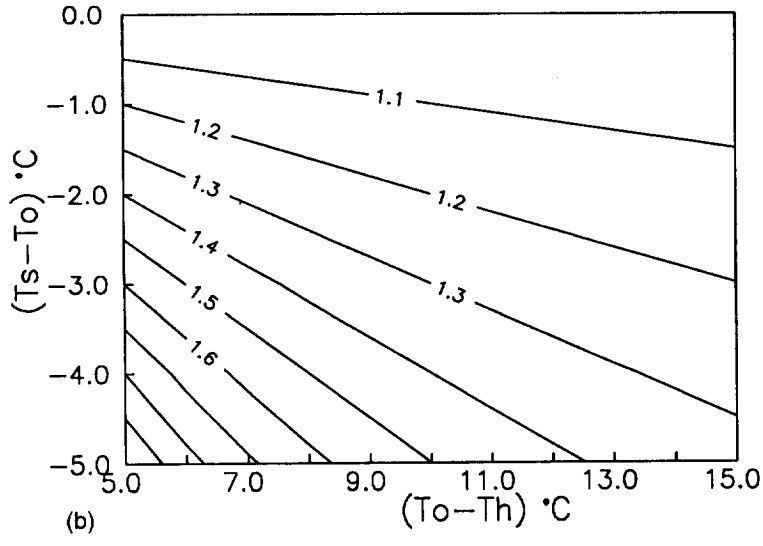


Fig. 2. (a) Obuchov's length scale(m) vs wind speed($ms^{-1}$): $L_h = \beta W^3/Q_s$ where; $\beta$ = 4.4893 $Joul.s^2.m^{-4}$, and $Q_s$ = 160 $Joul.m^{-2}s^{-1}$, (b) SST difference vs temperature jump value and $L_h/h_o$ parameter (shown by isolines): $(T_s - T_0) = (1 - L_h/h_0)(T_0 - T_h)$ considering $h_0 \leq L_h$ and $T_h \leq T_s \leq T_0$.

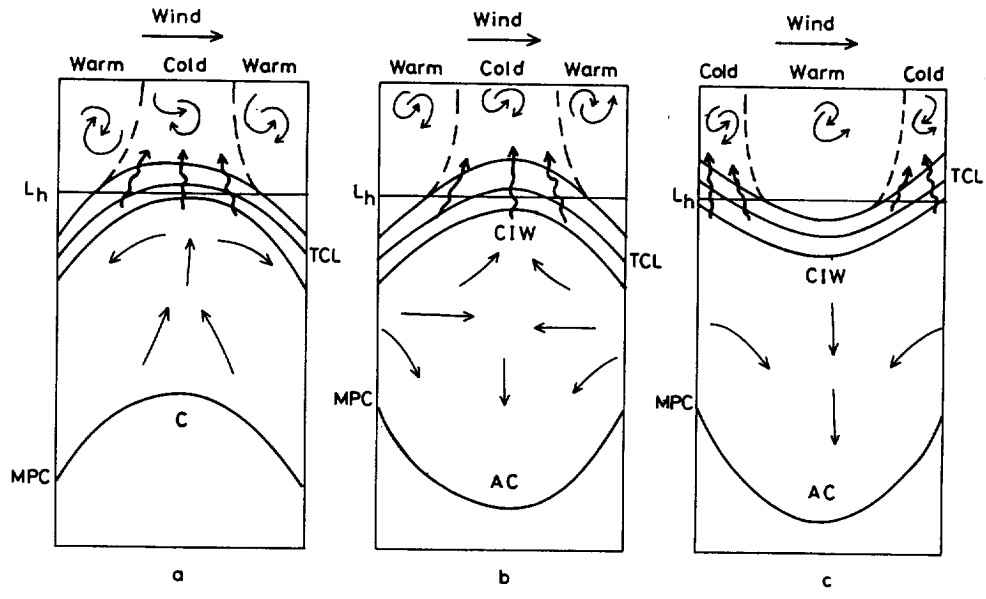


Fig. 3. Surface feature formation scheme under turbulent entrainment mechanism in the different stratification conditions: (a) cyclone; (b, c) anticyclone in summer and early autumn respectively. Notations used: TCL - seasonal thermocline; MPC - main picnocline; CIW - cold intermediate water; arrows - water movement directions; wawy arrows - turbulent entrainment in upper mixed layer.

Obviously, in nature, all of the mechanisms affecting the surface temperature field act simultaneously. For example, whenever the temperature anomaly at the surface is produced by entrainment, the horizontal gradient in $T_s$ develops and then action of the advection mechanism starts to be observed. It tends to change isotherm configurations as mentioned above, then the vorticity sign in anticyclonic or cyclonic cold anomalies are identified.

In the next section we will display results of mesoscale motions recognized in real satellite scenes. For their description, it will be of use to refer to results stated above.

## 4. MESOSCALE VARIATIONS IN DIFFERENT REGIONS

### *4.1. The Kerch region*

During the HydroBlack-91 (September 1991), the clearest pattern observed in the region south of the Kerch Strait was a large anticyclonic meander with dipole eddies on its termination. Dynamical topography maps have also shown the same structure within the whole water column over the main halocline (OĞUZ *et al.*, 1994). Since the hydrographic data are not synoptic and show rather complicated space-time dependent variations, especially for the upper layer because of significant seasonal and diurnal thermal variability occurring in late summer early autumn, a series of AVHRR images enable us to investigate the time evolution of this pattern.

Before September, a strong surface meandering feature and an anticyclonic eddy is observed

on the thermal images of August, 1991 (Fig. 4a–c). A large anticyclonic curling feature to the south of the Taman peninsula is clearly seen in the images of the 12th, 16th and 17th of August 1991 in spite of relatively low horizontal thermal contrasts. The dimension of the closed cold anomaly at the vortex center was ≈ 60 km along-meridian and ≈ 30 km along-parallel. This cold spot can be explained by the turbulent entrainment mechanism described in the previous section. The temperature difference between central and peripheral surface waters ranged from − 0.8 to − 2.7°C during the August satellite observations. Between August 17th and September 6th, thermal contrasts increased as a result of the onset of the cooling season, and the southern end of the meander had been displaced westwards (Fig. 4c,d). Progress of the feature towards the west continued until September 25th (Fig. 4c–h). The entire path of displacement was ≈ 125 km on the southern termination and ≈ 35 km on the shore-side of the meander. The average westward movement speed of the meander was about 3.5 and 1 cm.s$^{-1}$ along the southern and northern edges respectively.

All of the images from the 14th until the 25th of September 1991 showed a warm filament along the eastern edge of the cold feature with temperatures exceeding that of surrounding water by about 2°C. This filament was also reported by OĞUZ *et al.* (1994), who described the dipole eddy structure located north-west of the filament which corresponds to the anticyclonic Crimean eddy, following the terminology used by OĞUZ *et al.* (1993), and the cold surface spot south-east of the warm jet corresponds to the cyclonic eddy near the northern boundary of the eastern basin gyre (Fig. 4i). Formation of the surface patterns over these quasi-permanent circulation elements can easily be observed in successive satellite images; for example, anticyclonic eddy development is clearly pronounced at the surface in the pictures of 14th and 15th September 1991 (Fig. 4e,f).

Satellite images from summer 1992 (Fig. 5) display different mesoscale dynamics patterns from those seen in summer 1991, as discussed above. First of all, the warm band of the meandering Rim Current jet is remarkably well defined. The wavelengths of these meanders ranged between 78 and 88 km from May to August. This wave-like structure is sometimes complemented by eddy features both cyclonic (to the left of the jet) and anticyclonic (to the right), the latter being the more pronounced. Consideration of the picture sequences from May 21st to August 3rd (Fig. 5a–f) give us information about the progress of the eddy-meandering system. The strongly defined anticyclonic feature south of the Kerch Strait, with dimensions of 45 km along meridian and 65 km along parallel, was displaced 10 km southward between May and June, and its dimensions were transformed to 65 and 37 km respectively (Fig. 5a,b). Then within 12 days it moved 55 km westward (Fig. 5b,c) with a speed of 4.5 km/day ( ≈ 5 cm.s$^{-1}$). Later, from July 7th to August 2nd, its westward movement slowed to 2 km/day. Note that the contrast of cold surface anomaly at the center of this anticyclonic feature (maximal $\delta T_s \geq 2$°C in July) had nearly the same magnitude in July 7 and August 2,3 (Fig. 5c–e).

The presence of the meandering Rim Current and anticyclonic eddies with an enclosed cold spot were confirmed by hydrographic data, obtained in July 1992 during the CoMSBlack cruise (Fig. 5h–j). On the other hand, higher amount of surface heating throughout the whole area during August diminished thermal contrast at the surface, so that in August 10 and 15 1992 the only feature revealed was a long-wave meander of the Rim Current (Fig. 5f,g).

In the scene of 21 May 1992, different-scale wave structures are revealed (Fig. 5a). The long-wave meanders were accompanied by short-wave ones on the shore side of the Rim Current. Mean wavelengths were about 37 km but decreased individually from east to west. Such estimates are evidence of the simultaneous presence of two wave systems formed by instability mechanisms, both barotropic (long-wave pattern) and baroclinic (short-wave one), of the shear

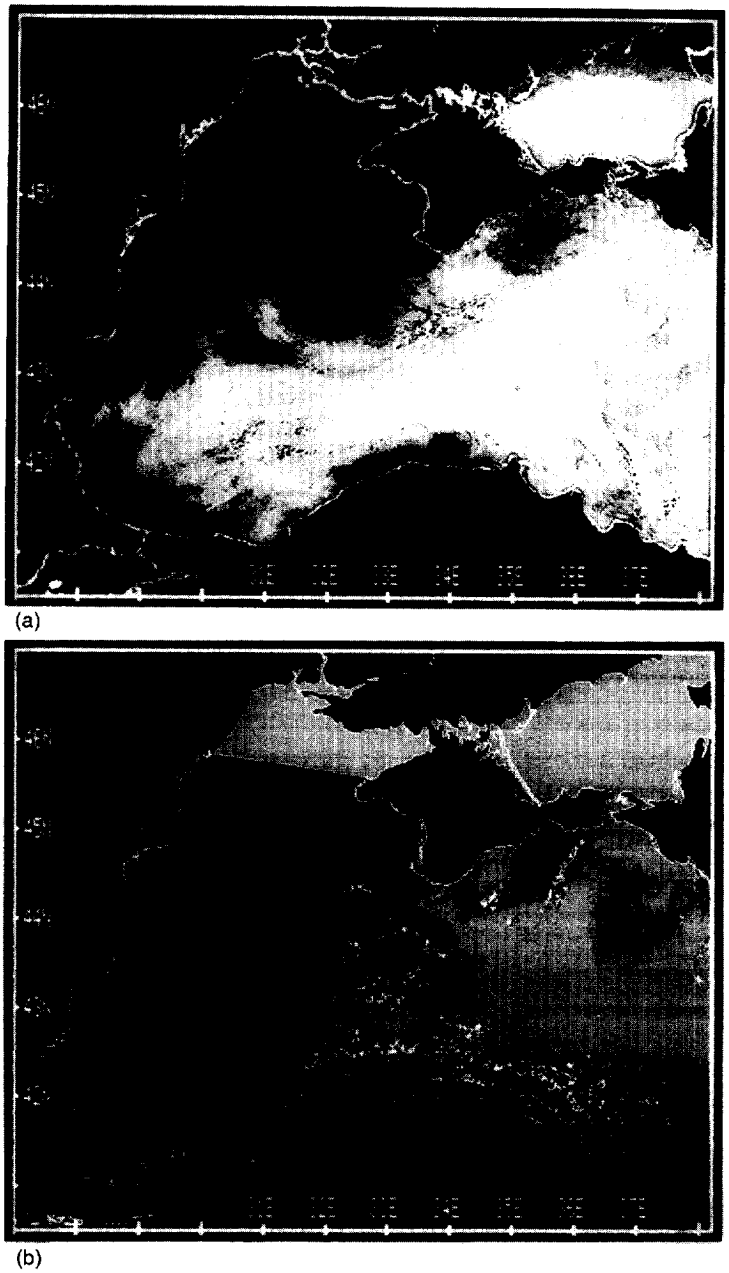


Fig. 4. Infrared image sequence in 1991; (a–c) August 12, 16, 17 and (d–h) September 6, 14, 15, 18, 25, and (i) Dynamical topography maps of the September/HydroBlack-91 cruise. (In this and the following thermal images, the darker tones represent colder and the lighter tones represent warmer water).

(c)

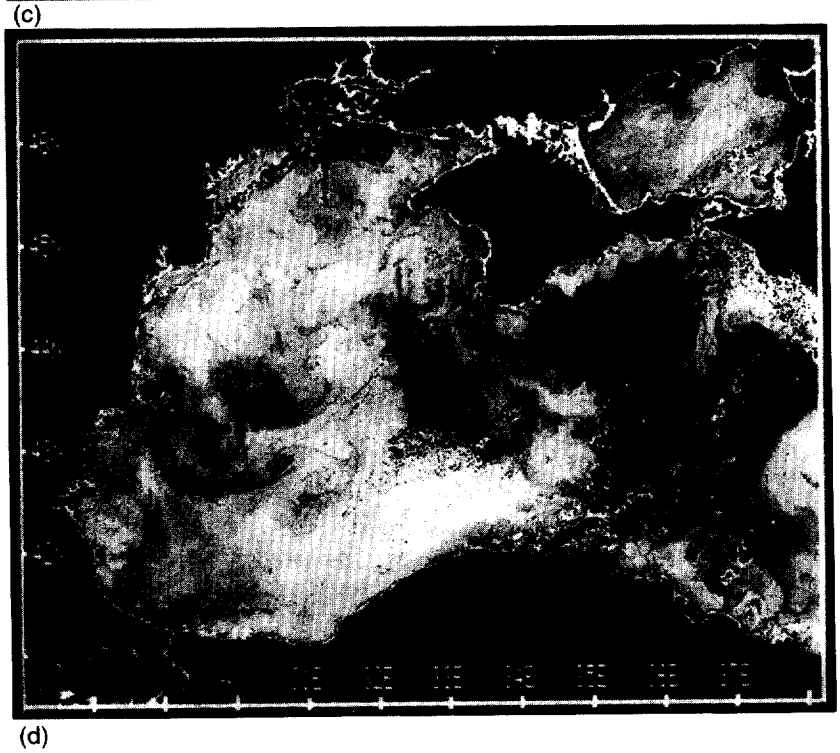

(d)

Fig. 4. Continued

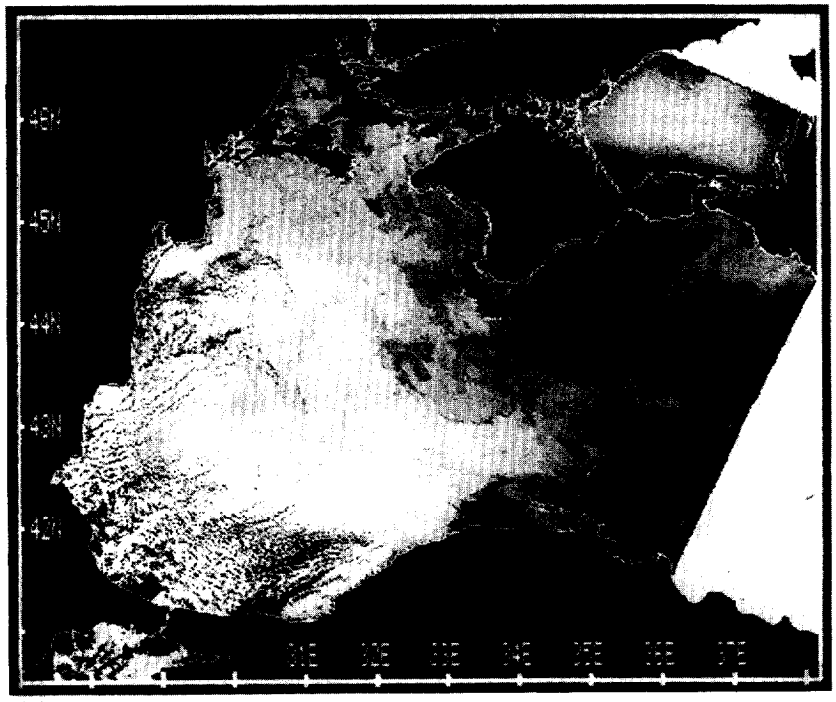

(e)

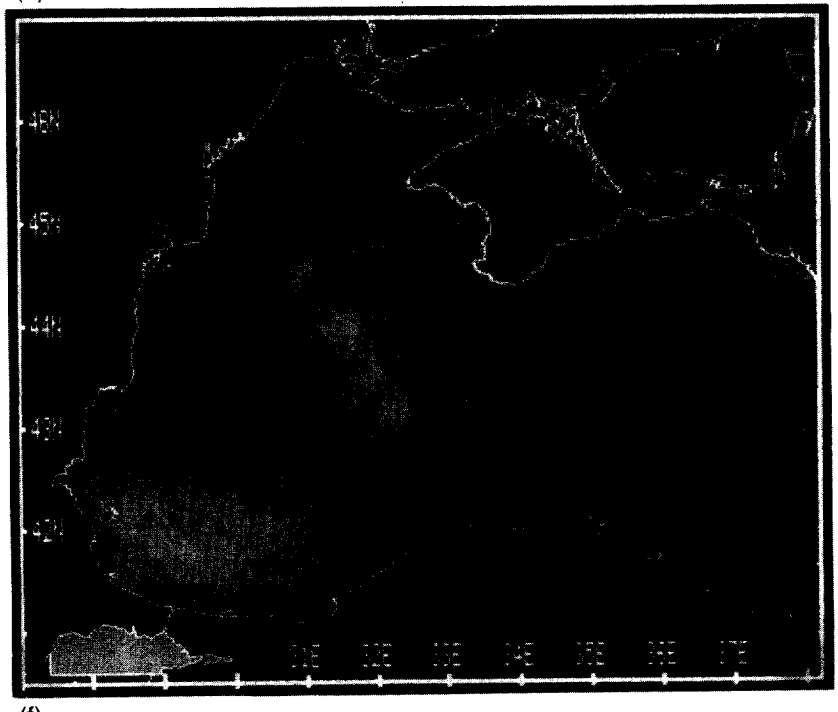

(f)

Fig. 4. Continued

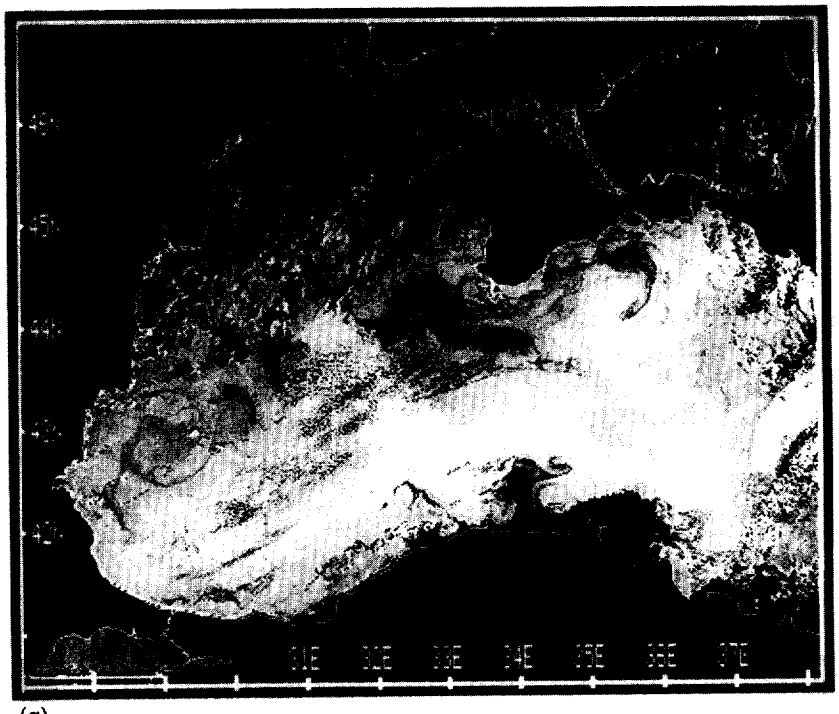


(g)

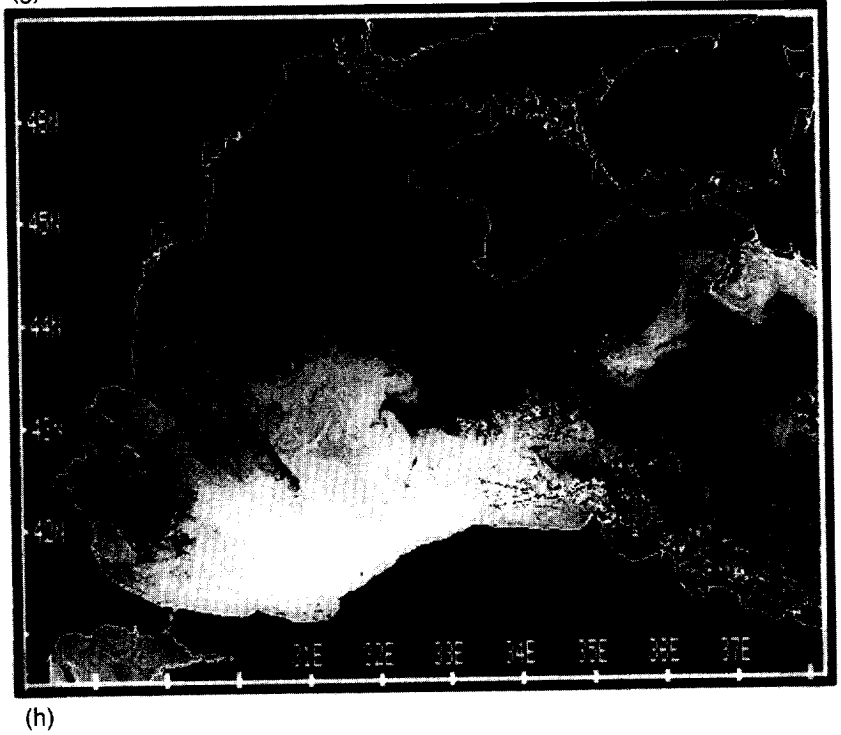


(h)

Fig. 4. Continued

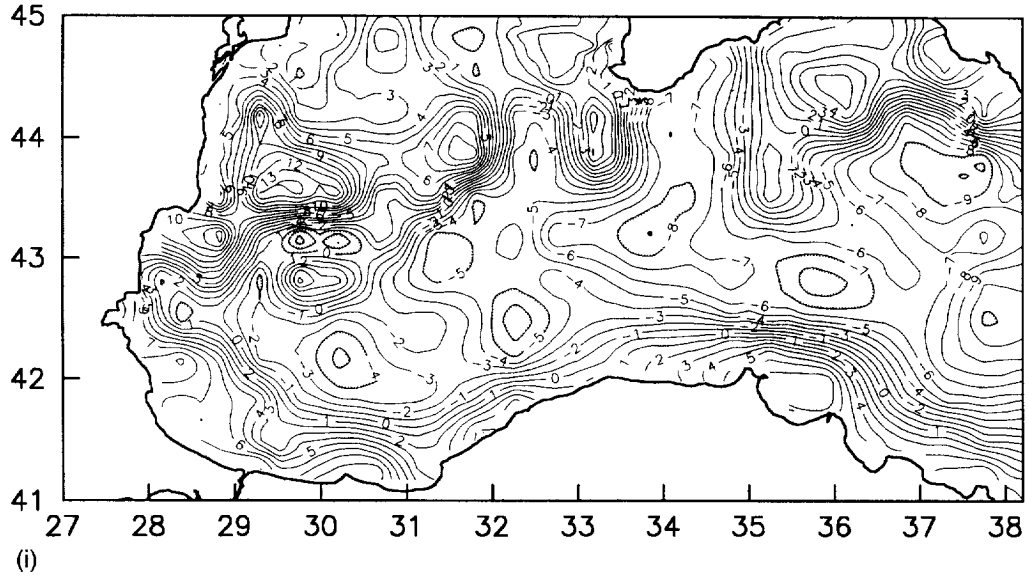


Fig. 4. Continued

current along the shelf-break. Evidence of a similar structure was obtained earlier by means of empirical orthogonal function analysis of the time series of daily received thermal APT images in summer 1991 (IVANOV and ILYIN, 1993), where an example of a two-wave structure was visualized in the presence of strong cross-isobath temperature gradients. On September 6, 1991; only the short-wave system is clearly seen (Fig. 4d), where wave-like meander has $\approx$ 35 km wave length along the coastal warm water front. Quantitative estimates for the wavelengths obtained both here and in Ivanov and Ilyin's (1993) work are in good agreement, the latter being confirmed by corresponding theoretical dispersion equations following barotropic and baroclinic instability models.

### *4.2. Western region*

The western part of the Black Sea displays the formation of the mesoscale circulation features become notable under specific conditions. Besides the instabilities of the Rim Current, the thermal processes in the shallow north-west shelf and freshwater outflows of the main rivers (Danube, Dnieper and Dniester) are the sources of horizontal inhomogeneities in the density structure. These processes generate strong signals in the satellite observations of the water dynamics in the infrared band (GRISHIN *et al.*, 1989a, b; ILYIN and GRISHIN, 1992; SUR *et al.*, 1994, 1996).

During the spring-summer period, turbid low salinity waters were apparent on the images because of their higher absorption of the sun's energy and relatively faster heating in comparison with the surrounding transparent surface seawater. Shelf water increases in density as it cools in winter and slips down the slope under the gravitation force, together with the waters from cold centers of the cyclonic gyre domes, where it is accumulated in the convergence zone at the shelf break (IVANOV, 1992). This process promotes the intensification of anticyclonic eddies on the right hand side of the Rim Current (LATUN, 1990). It also determines the thermal charac-

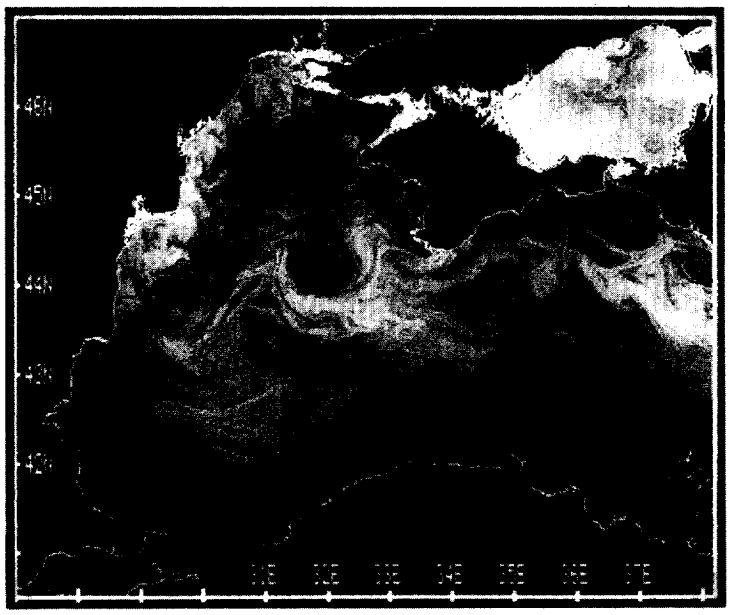

(a)

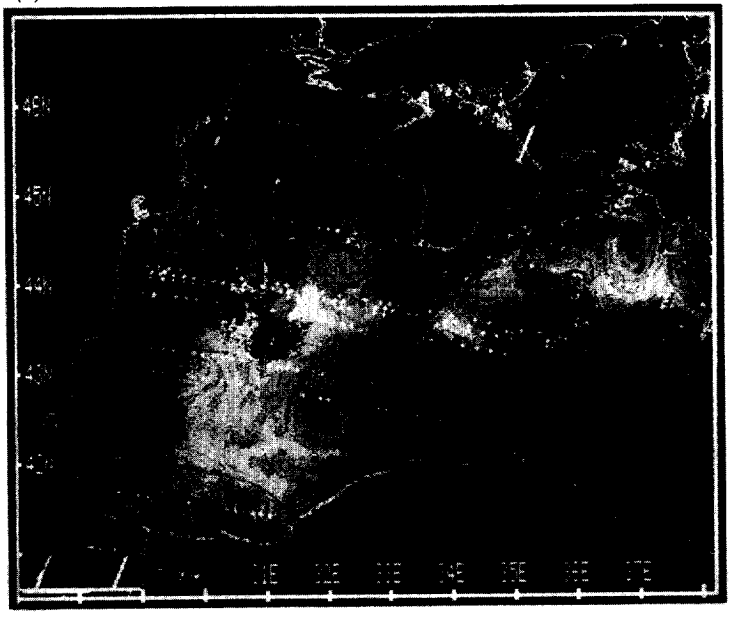

(b)

Fig. 5. Infrared images in 1992; (a) May 21, (b) June 24, (c) July 7, (d–g), August 2, 3, 10, 15; (h–j) Dynamical topography, surface temperature and salinity maps of the July / CoMSBlack-92 cruise.

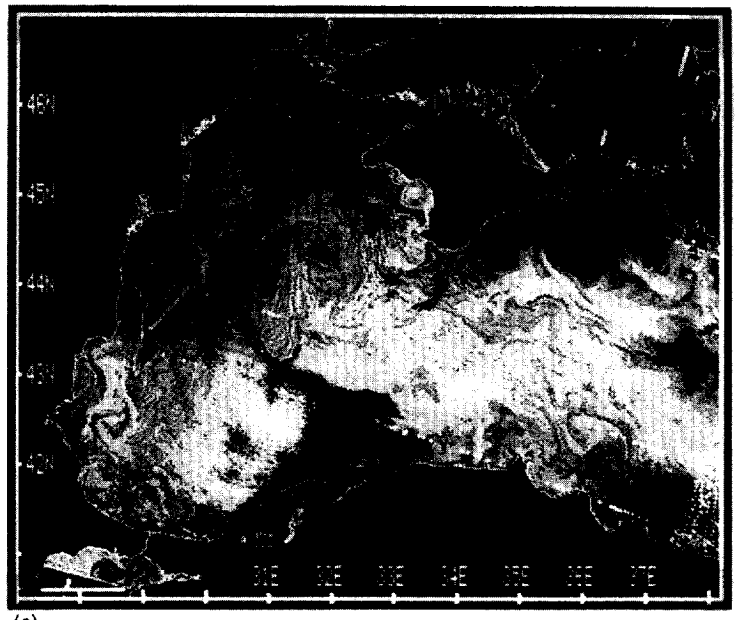


(c)

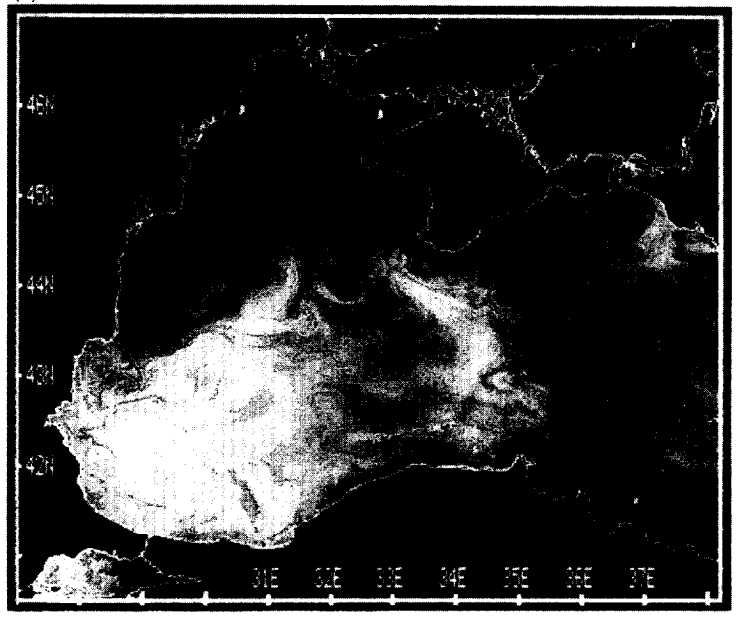


(d)

Fig. 5. Continued

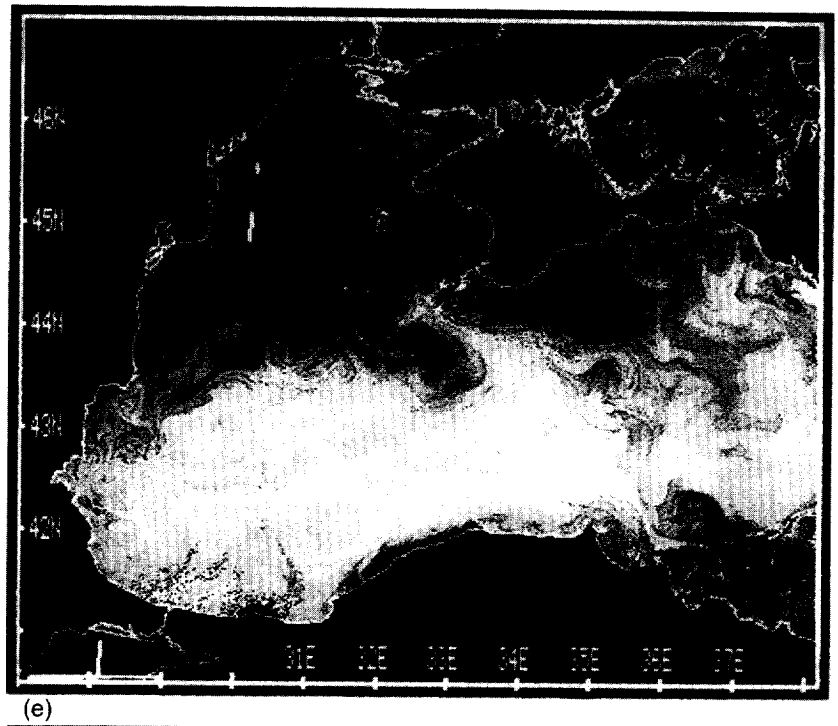


(e)

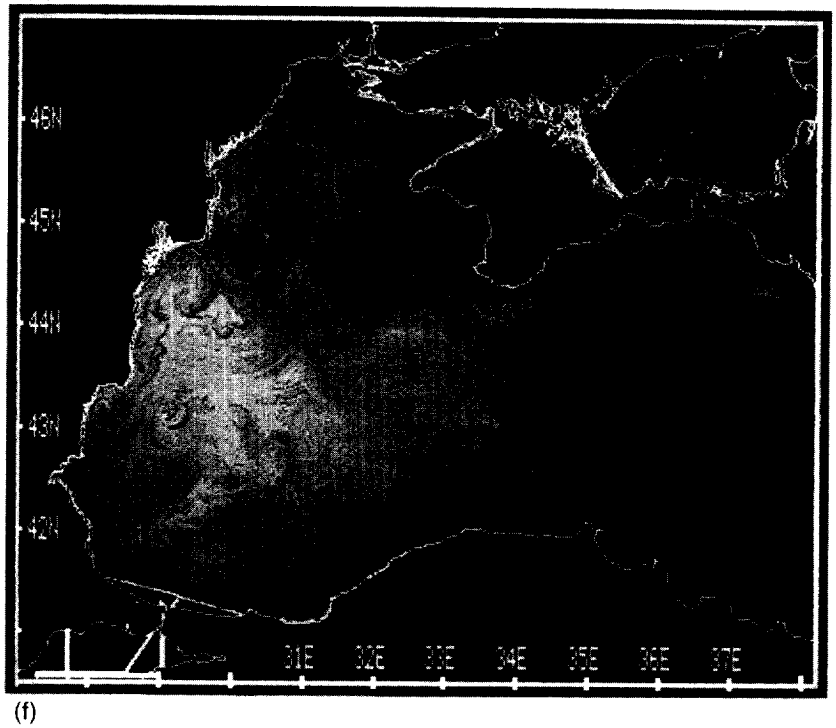


(f)

Fig. 5. Continued

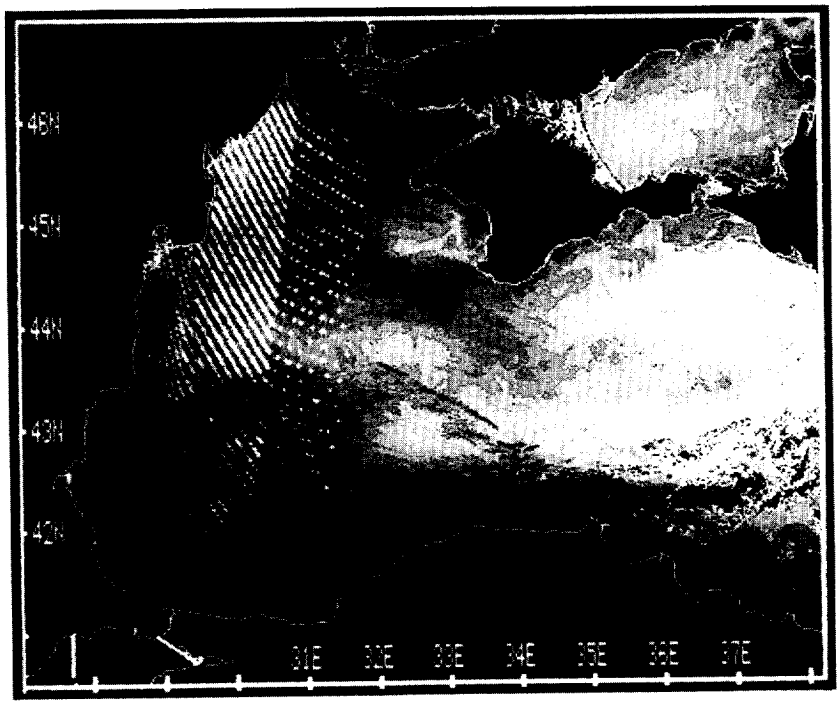


(g)

Fig. 5. Continued

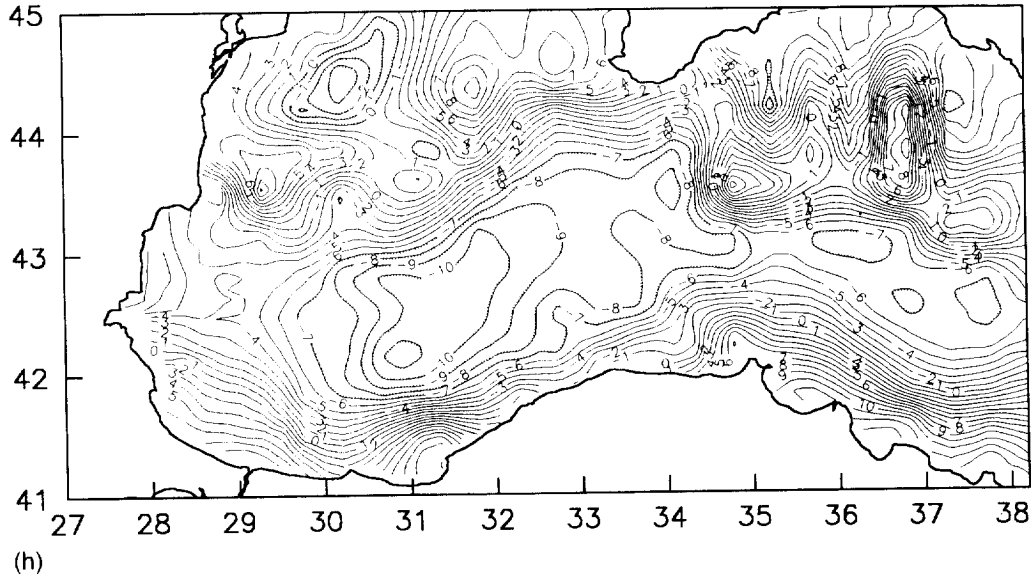


(h)

Fig. 5. Continued

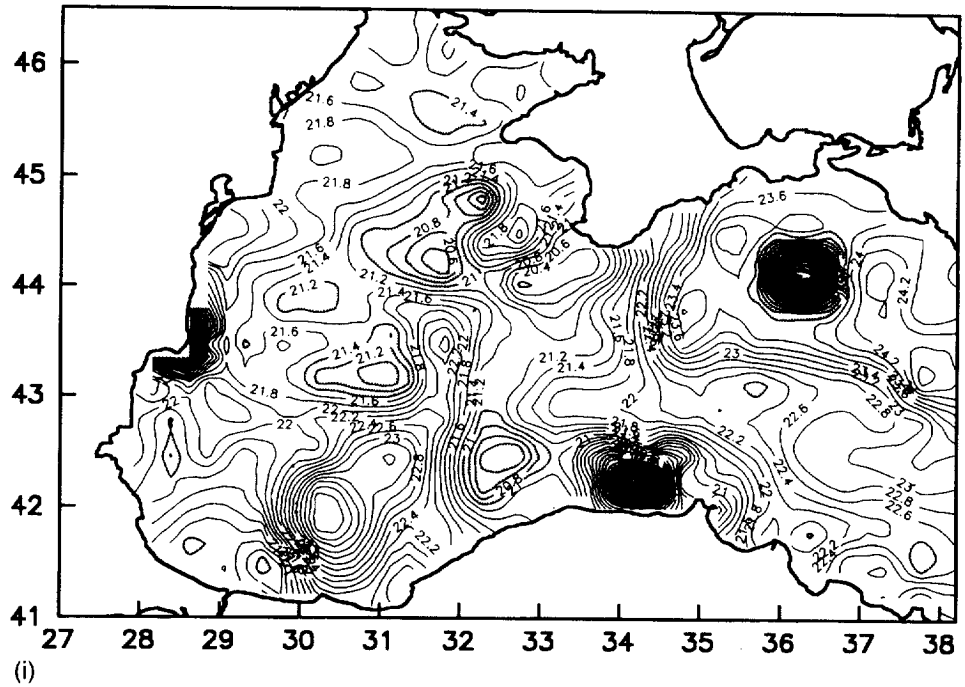


(i)

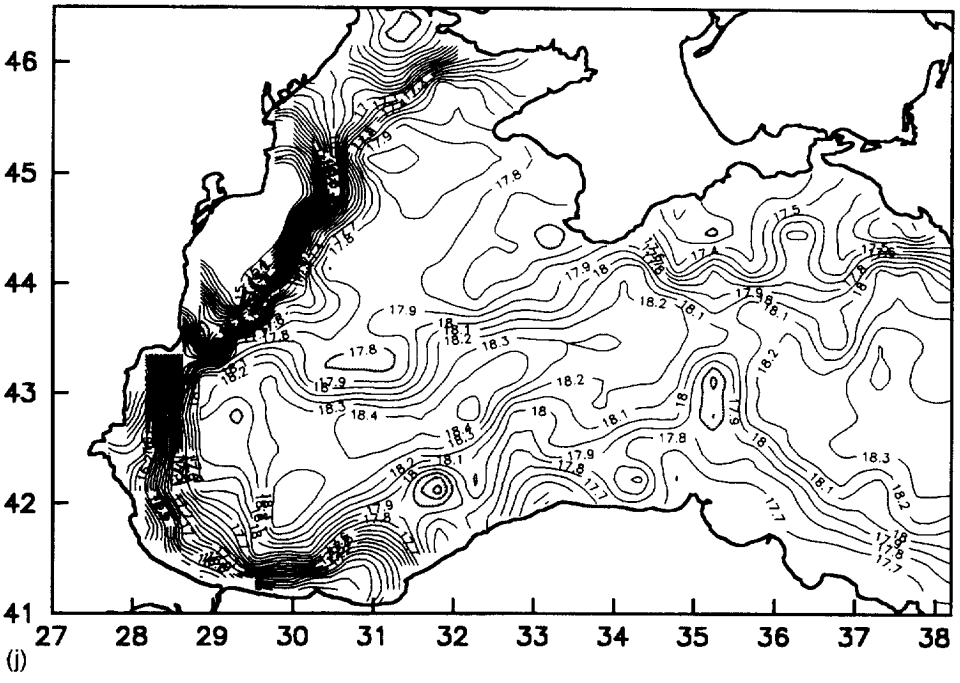


(j)

Fig. 5. Continued

teristics of the vertical structure of the anticyclones which, as mentioned in Section 3, have cold anomalies at their centers.

The most studied quasi-permanent features in this region are the anticyclonic gyre to the south-west of the Crimean peninsula, the so-called "Sevastopol eddy" (following terminology used by OĞUZ *et al.*, 1993), and the "Kaliakra eddy" to the south-west of it. These eddies sometimes contain more than one core, which may be intensified and slightly shifted in their locations but remain within the usual limits of the anticyclonic gyre.

Surface manifestations of quasi-stable mesoscale events undergo significant seasonal and synoptic changes. Their nature depends at first on the vertical stratification of the water column and wind fluctuations. Typically, both local mechanisms (solar heating and turbulent entrainment) and the variable advective processes (development of vergence zones and mushroom-like currents) are observed in this region. In Table 1, locations and dimensions of the surface patterns related to the main quasi-permanent eddy events at the shelf break as evaluated from the satellite images of 1991 and 1992 in summer are listed. Horizontal differences in surface temperature between the eddy centers and peripheries are also given in the same table. It is clear in this table that the shelf core of the Sevastopol eddy is always warmer than the surrounding waters, and that western and eastern (deep-water) cores of this eddy become warmer by the end of the summer. The "Kaliakra eddy" is distinguished only in some images; August 17,19 and September 6 of 1991 (Figs 4, 6a and 4d); July 3,7, August 2 and September 3 of 1992 (Figs 7a, 5c,d and 7d), and also shows a negative surface anomaly.

In the light of the hypothesis concerning the influence of the seasonal evolution of CIW on the vertical and surface structure of an eddy (Section 3), the temperature anomalies on the infrared images near the Sevastopol region can be explained in the following manner: In shelf regions the anticyclonic gyres are not influenced by CIW as much as the deep-water cores,

Table 1. Quasi-permanent anticyclonic eddies in the western part of the Black Sea (satellite derived characteristics).

| Feature | | Longitude °E | Latitude °N | Diameter(km) | Temp.differ(Cent.-Periph.) | Time |
|---|---|---|---|---|---|---|
| Sevastopol | western core | 31.4–31.6 | 44.3–44.5 | 52–66 | − 0.5/ − 1.2 | August 1991 |
| eddy; | eastern core | 32.7–32.8 | 44.8 | 44–26 | − 0.3/ − 1.3 | |
| | shelf core | 33.2–33.3 | 44.7 | 27–37 | + 0.3/ + 0.5 | |
| Kaliakra eddy | | 30.2–30.3 | 43.3–43.4 | 60 | − 0.5/ − 0.7 | |
| Sevastopol | western core | 31.6–31.9 | 44.6–44.7 | 55 | + 0.4/ + 0.6 | September 1991 |
| eddy; | eastern core | 32.6–32.8 | 44.8–44.9 | 52 | + 0.4/ + 0.5 | |
| | shelf core | 33.2–33.3 | 44.7 | 22–33 | + 0.5/ + 0.6 | |
| Kaliakra eddy | | 30.5 | 43.4 | 63 | − 0.5/ − 1.0 | |
| Sevastopol | western core | 31.7–32.1 | 44.2–44.4 | 74–42 | − 0.5/ − 0.8 | May–Aug. 1992 |
| eddy; | eastern core | 32.5–32.7 | 44.7–44.8 | 25–30 | − 0.5/ − 1.0 | |
| | shelf core | 33.1–33.3 | 44.3–44.9 | 37–55 | + 0.7/ + 1.2 | |
| Kaliakra eddy | | 30.3–30.5 | 43.6 | 75–85 | − 0.5/ − 0.7 | |
| Sevastopol eddy | | 32.1–32.2 | 44.5–44.6 | 65 | + 0.5/ + 1.5 | September 1992 |
| Kaliakra eddy | | 30.1 | 43.6 | 60 | − 0.8/ − 1.0 | |

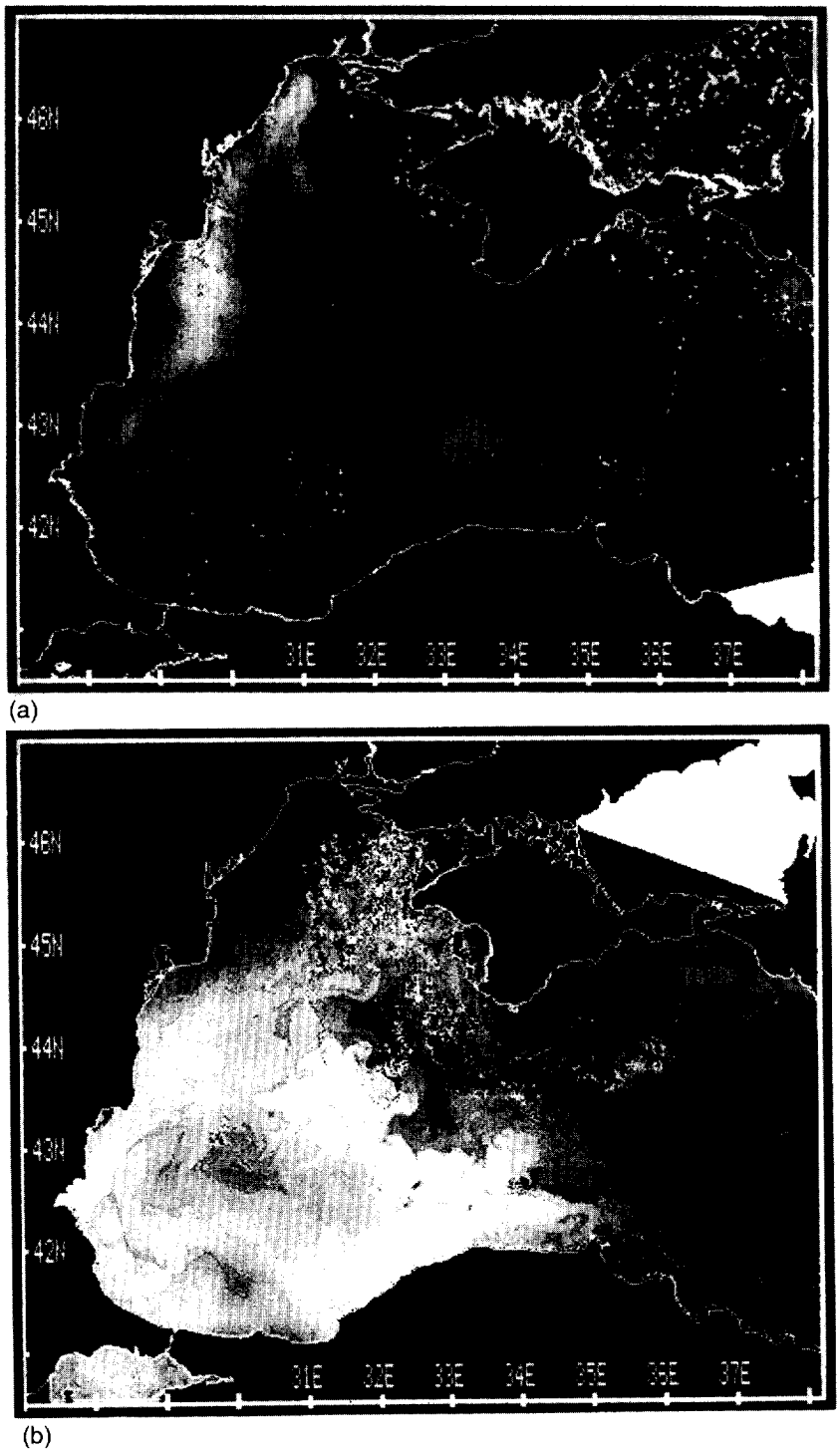


Fig. 6. Infrared images in 1991; (a) August 19, and (b) September 24.

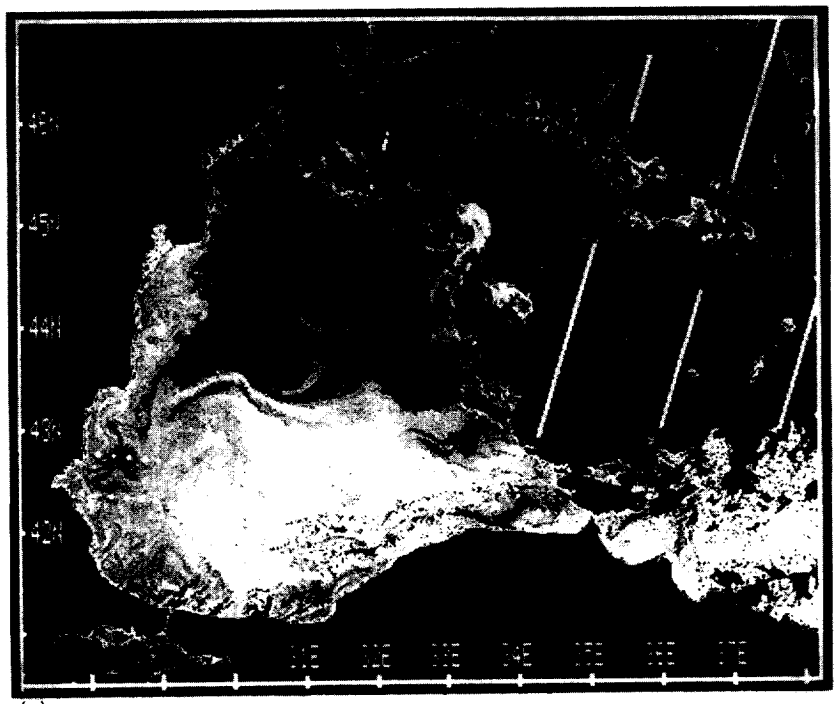


(a)

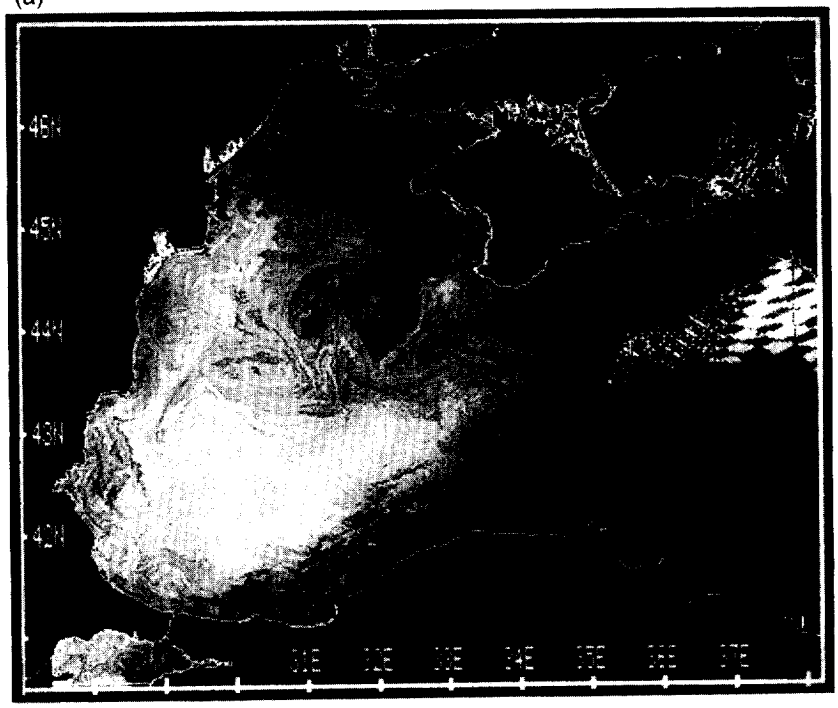


(b)

Fig. 7. Infrared images in 1992; (a,b) July 3,6, (c) August 12, and (d,e) September 3, 5.

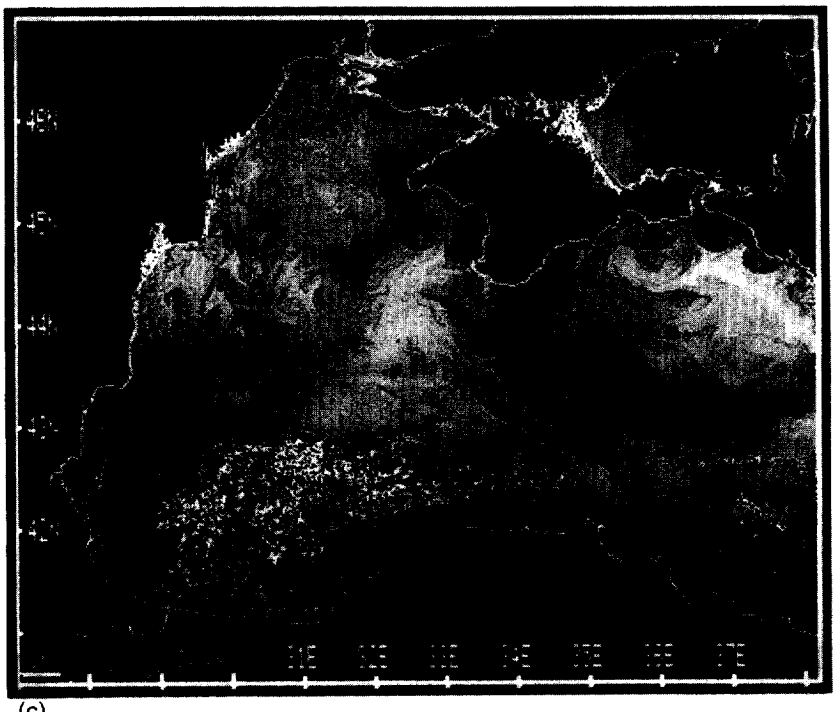

(c)

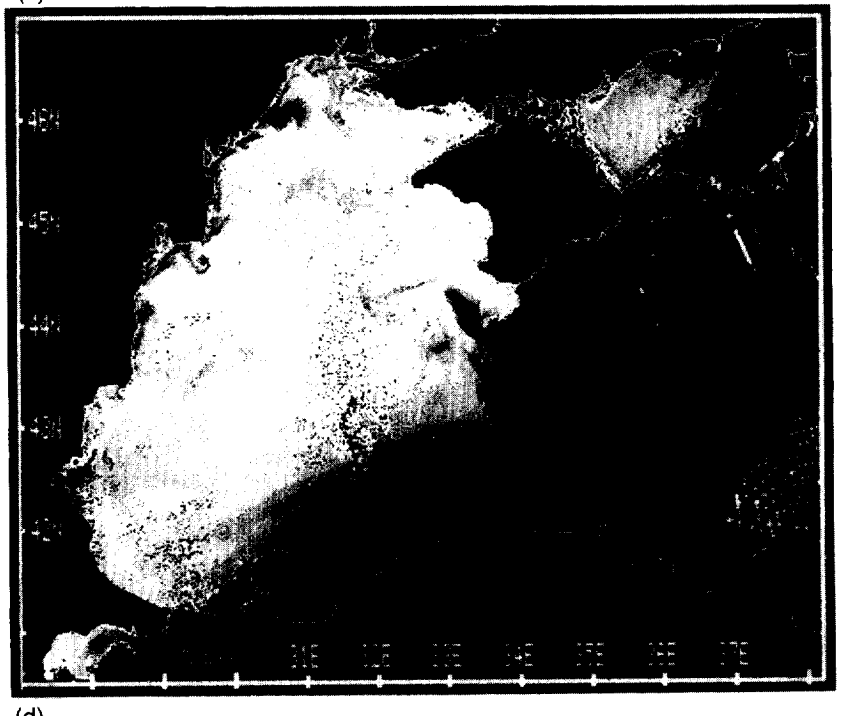

(d)

Fig. 7. Continued

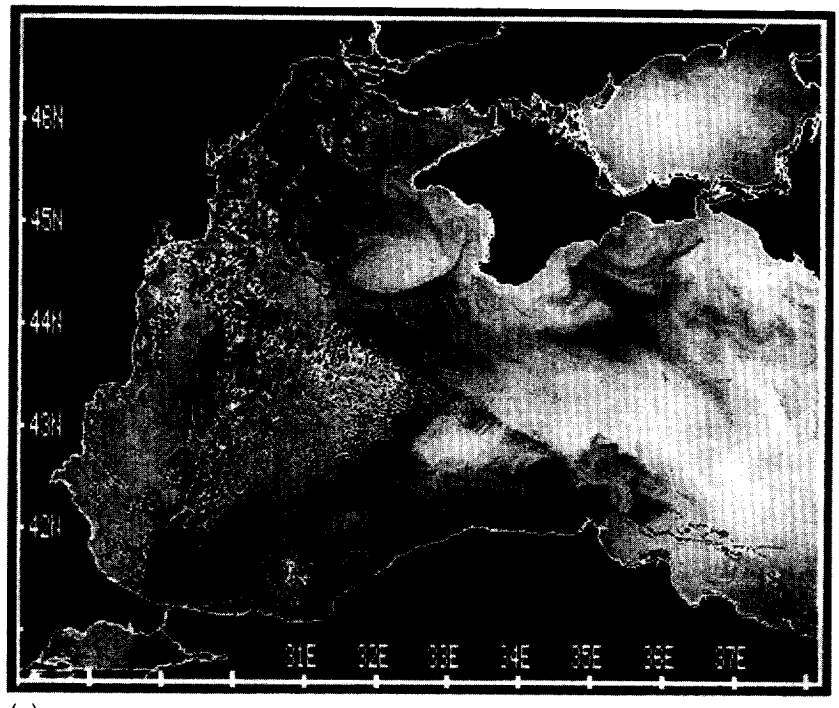


(e)

Fig. 7. Continued

therefore the convex structure of the seasonal thermocline is not expressed within the eddy centers on the shelf during summer. Anticyclonic convergence leads to the accumulation of warm surface waters as shown in Fig. 3c. The same situation occurs within the cores of deep-water eddies but only at the end of summer when the fresh ingresses of CIW are halted and its surpluses are advected away by the Rim Current to the south-west. The chain of anticyclones on the right-hand side of the Rim Current act as a pump system which handles CIW waters subsequently. Therefore, in the Kaliakra eddy, the thickness of CIW decreases later than in Sevastopol eddy, and also the surface anomaly contrast becomes positive with time.

The vertical thermal structure and evolution of the surface pattern for the western core of the Sevastopol eddy is demonstrated by way of *in situ* data from the hydrographic surveys in May, July, August and October of 1992. Figure 8 shows the temperature cross-sections through the eddy centers (note the ship's track did not cut across the whole eddy but terminated at its center in May). In late spring, the usual anticyclonic pattern of the main isotherm was observed (Fig. 8a); lower and upper boundaries of the CIW (the lower and upper 8°C isotherms, respectively) had deepened at the eddy center, i.e., the filling of the anticyclone by cool shelf waters was at an early stage. In the upper part of the seasonal thermocline some spreading of the isotherms occurs probably as a result of the advection of surface water from the north western shelf (NWS), therefore, the cold anomaly over the anticyclone is unrelated to the CIW effect. At the beginning of July, the upper boundary of CIW in the eddy core was domed (Fig. 8b), and the seasonal thermocline was pushed up closer to the sea surface. This facilitates the formation of cold anomalies as a result of turbulent entrainment (see Fig. 3b). The same situation persisted

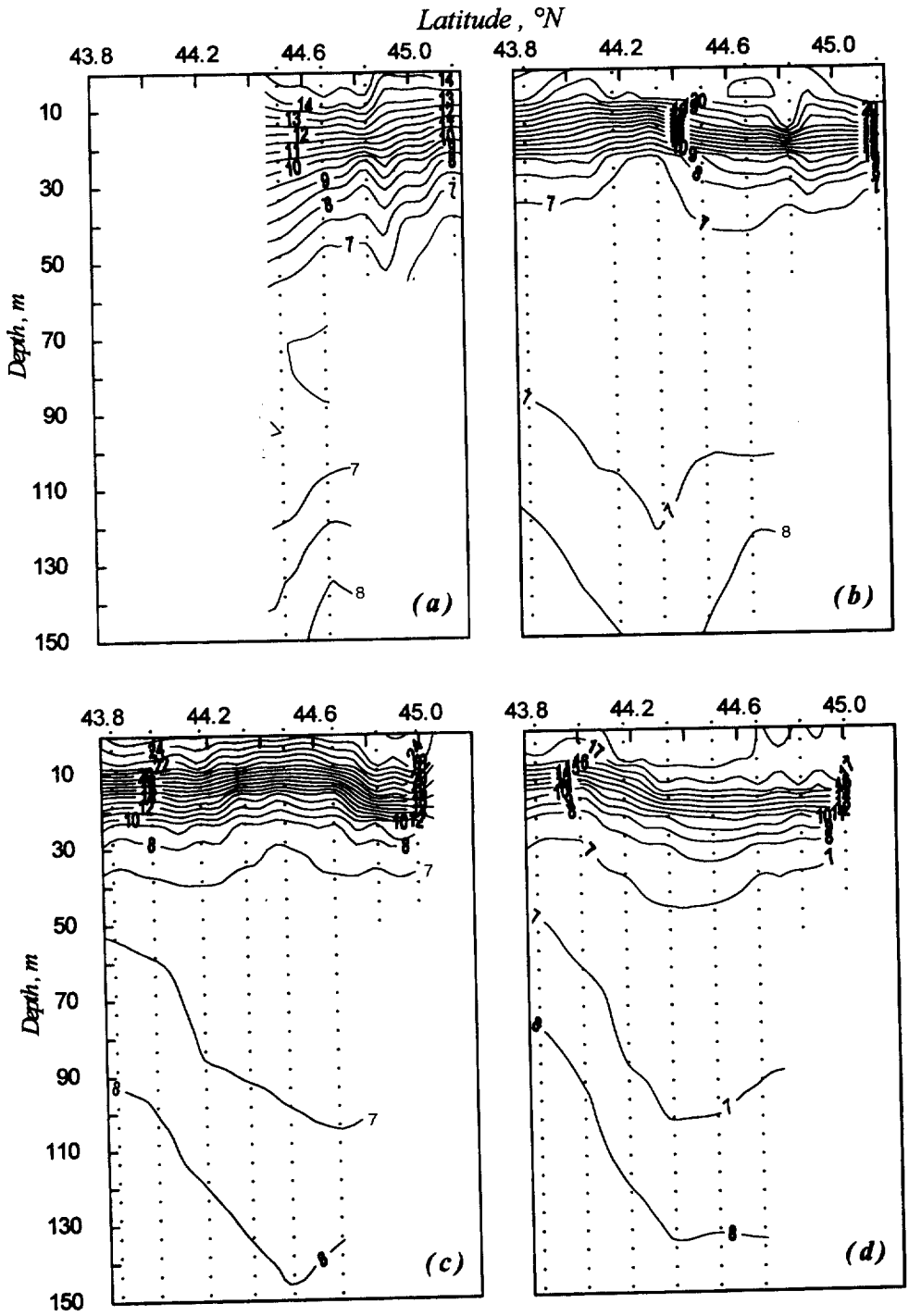


Fig. 8. Meridional temperature sections across the Sevastopol eddy western core (31.70°E) during 1992 surveys: (a) May, 22–23, R/V "*Trepang*"; (b) July, 7–12, R/V "*Professor Kolesnikov*"; (c) August, 10–11, R/V "*Yakov Gakkel*"; (d) October, 2, R/V "*Mikhail Lomonosov*".

into August (Fig. 8c). The warm anomaly over the Sevastopol eddy which was observed in September, 1992 (Fig. 7d,e, Table 1), was probably caused by a decrease in the CIW thickness and the deflection of its upper boundary, as is observed along the cross-section for the beginning of October (Fig. 8d).

The data presented confirms the scheme considered in Section 3 (Fig. 3b,c). We can see from Table 1 and Fig. 8, that the typical value of $(T_s - T_0)$ is about $-1.0$°C and that of $h_0 \approx 8 - 12$ m. The limits of $(T_0 - T_h)$ are 9–12°C. Using these values we can find from Fig. 2b that the parameter $L_h/h_0$ ranges between 1.08–1.12, and $L_h \approx 9$–13 m. Thus, it is enough for the scale of penetration of vertical turbulent mixing to be only 1 m larger than $h_0$ for the turbulent entrainment mechanism to occur and result in the occurrence of thermal anomalies over the Sevastopol anticyclone. In Fig. 2a, a wind speed about 7–8 m.s$^{-1}$ corresponds to the obtained value of $L_h$ which is in agreement with the observations.

Mesoscale features, having time scales of several days, are caused by variability processes in the upper part of the baroclinic layer (mixed layer and seasonal thermocline). The main reasons for the occurrence of the thermal inhomogeneities are divergences resulting from unstable wind induced currents or impulses of wind acting on the sea surface, as well as buoyancy flux effects as a consequence of both river run-off and solar heating of the upper mixed layer. Besides these events, vertical thermal convection at the beginning of autumn intensifies the horizontal contrasts of SST which further induces additional eddy movements in the upper layer. The most characteristic manifestations of aperiodic mesoscale motion are the bands of cold upwelled waters near shorelines. FEDOROV and GINSBURG (1989) stated that cold cross-jets (filaments) and spots at divergence zones in the open sea, mushroom-like currents, as well as meanders and eddies are formed as a consequence of barotropic and baroclinic instabilities of the Rim Current.

In August 12, 1991; a cold anomaly was observed to the north of the Sevastopol divergence region. Cold water from this anomaly was being entrained into the core of the western gyre (Fig. 4a). Five days later, an eddy-like cold anomaly appeared on the cyclonically meandering crest. This anomaly seems to have been related to eddy formation resulting from the current's instability (Fig. 4c). In both this image and the following one, warm waters can be traced extending from the mouths of the Danube and Dniester Rivers not only towards the south (along the western coast) but also towards the east (Fig. 4c,Fig. 6a). During the spreading of this warm water, mesoscale eddies (diameter of 15–30 km) are formed, with the tendency for cyclonic curling. Horizontal turbulent processes seen in these images occur under the influence of westerly winds, evidence for which is seen in the band of cold water extending along the western coast (Fig. 6a), since the warm river waters are pushed eastward to the shelf break and then transported southwards by the Rim Current. Some parts of this band are entrained into the Sevastopol gyre zone and advected south between the cyclonic meander and the western anticyclonic core of the Sevastopol Gyre.

In May 1992, the influence of the riverine waters to the western shelf could be traced even more distinctly during the maximal outflow after the spring flood (Fig. 5a), and various eddies with diameters of 15–20 km were observed along the plume. In summer 1992, the Danube waters, which were 0.5–1.0°C warmer than the surroundings, extended across the shelf region and were entrapped by anticyclonic eddies at the shelf break (Fig. 7a,b,c). At the same time both warm and cold cross-jets extending from the west coast towards the east were observed which terminated in cyclonic vortexes indicating the cross-flow of the alongshore current in a south-west direction (Figs 5g and 7c,d).

Examples of cold anomalies at the current divergence zone are also seen in the images of

July 3, September 3 and 5 of 1992 (Fig. 7a,d,e). In July, the divergence is seen as a cyclonically meandering foot between the western and eastern cores of the Sevastopol anticyclone, where the surface water was cooler than the surrounding water by about 2–3°C. The September images show the divergence zone to the south-west of Crimea and cold filaments along the periphery of the Sevastopol anticyclone.

Another formation is exemplified by the mushroom-like structure seen in July 6, 1992 (Fig. 7b) at the termination of the cyclonic meander considered in the previous paragraph. The right hand side of this structure coincides with the quasi-permanent western core of the Sevastopol anticyclone. Another mushroom-like structure was observed on August 2, 1992, where the foot stretched from the upwelling area of the Crimean shelf to the south-west, the pair coincide with the anticyclonic and cyclonic eddies located on both sides of the Rim Current (Fig. 5d). The northern part of the mushroom's cap is terminated by another small scale dipole. Small-scale patterns were observed until August 12 on the periphery of the Sevastopol anticyclone (Fig. 5f,Fig. 7c), whereas the large-scale one disappeared after August 3 (Fig. 5e). The mushroom-like structure seen in Fig. 7b presumably developed as a result of instability in the cyclonically meandering motion, and the dipole formation seen in Fig. 5c was possibly caused by the advection of upwelled water trapped in the Rim Current. Both cases demonstrate that quasi-permanent mesoscale events play an important role in eddy pair formation and further evolution.

### *4.3. The Bosphorus and Sinop region*

The satellite image of August 12, 1991 (Fig. 4a) shows two cold regions along the Bulgarian and Anatolian coast (near Cape Kerempe) which possibly resulted from temporary upwelling events. Wind induced upwellings with strong surface temperature manifestation were frequently observed along the shallow western coast as a result of the westerlies in this season. The core of the cold upwelled water observed along the Bulgarian coast displaying a strong temperature gradient as this water was dispersed during its advection by the Rim Current along the Turkish coast, but remained clear as far as the Sakarya Canyon. In the same image the cold region around Cape Kerempe indicates a developed upwelling event in the same region as described earlier by SUR *et al.* (1994). This upwelling region extended offshore ( $\approx$ 50 km) and alongshore, and showed the development of a dipole structure west of Cape Ince with its anticyclonic part being more pronounced and having a diameter of $\approx$ 25 km.

Four days later (Fig. 4b), the region between Cape Kerempe and Cape Sinop had become warmer. This was possibly caused by the cyclonic and anticyclonic areas of the dipole eddy capturing warm water from offshore regions and advecting onshore. The cold water had extended up to Sakarya Canyon and so covered a larger area. Also note that, cold regions along the shallow western coast disappeared after a short period during which atmospheric condition settled down.

In Fig. 6a, the upwelling region had sub-divided into two parts near Cape Kerempe. Filaments with $\approx$ 70 km extensions originated from this region having more uniform temperature and showing anticyclonic tendencies as result of Coriolis effects and sheer by the eastward Rim Current. There is another cold structure which is separated from the Bulgarian coast by the warm Danube flow.

Seventeen days later, on September 6, 1991, another image (Fig. 4d) shows that the cold filaments near Cape Kerempe had disappeared and an S-like anticyclonic structure had appeared offshore of Cape Kaliakra. It seems that this S-shaped structure was combined with the western part of the anticyclonic Sevastopol Eddy observed on the previous image which had shifted ($\approx$ 100 km) south-eastward within 17 days. The same rate of advection for the eastern part of

the Sevastopol eddy was also observed in a south-easterly direction approximately 5 cm/day southward.

The striking feature seen in Fig. 4e is the filament ( $\approx$ 55 km long) emerging from the upwelling region east of Cape Kerempe. In just one day, between September 14 and 15, 1991, a large change occurred in the area covered by the upwelled water, as it extended both offshore and alongshore. The offshore filament between Cape Kerempe and Cape Ince extended $\approx$ 70 km (Fig. 4f). Cold water with a strong temperature gradient spread out as far as the Filyos River, and another cold filament, near the mouth of the River, extending $\approx$ 35 km offshore had also developed within one day. Note that a similar structure was observed at the same place one month previously (Figs 4a and 6a). Although the strength of the Kaliakra eddy had declined, its position is maintained in this image (Fig. 4f).

Behind the cloud cover near Cape Ince (Fig. 4g), a strong offshore filament to the west of the Cape can be seen at much the same position as it had been 3 days earlier. Its shape had evolved into more of a mushroom-type structure having an anticyclonic tendency and some small scale instabilities along its offshore boundaries. The possible cause of these squirts may have be a local wind patterns which could be seen in cloud structures on the image. The cold band of water along the coast extending up to Filyos River had nearly disappeared except in the small area west of Cape Kerempe. The Kaliakra Eddy remained present but its position had shifted ( $\approx$ 20 km) southward.

Along the Anatolian coast the upwelling region disappeared within six days (Fig. 6b), as also shown by the hydrographic data taken during the latter part of September 1991. The *in situ* surface temperature distribution (SUR *et al.*, 1994) showed warm water along the coast in the recirculating area east of Cape Ince, except between Cape Baba and Cape Kerempe where the Rim Current is discontinuous, as shown by the streamlines in Fig. 4i. This region of discontinuous currents could, indicate either a coastal attachment of the current which was insufficiently resolved by the geostrophic analyses, or there was residual downwelling/upwelling along the coastline, although the transient events were observed somewhat earlier (SUR *et al.*, 1994).

Analyses of the hydrographic data covering the whole of the Black Sea made by OĞUZ *et al.* (1994) showed filaments occurring along the southern coast which were determined by extensions of low salinity water reaching the interior region. The coastal water in the region of the filaments was warmer than the central region of the Black Sea; a feature which was also observed in the September 24, 1991 image. Within a week, the cold Kaliakra Eddy had extended to cover a large area including the Bosphorus and Sakarya Canyons (Figs 4g and 6b). This large region was connected to the cold water on the north west and Crimea shelf, and thus to eastern Black Sea. One day later, as seen in Fig. 4h, there had been some very rapid changes; a region of warm water had extended westward to cover the Bosphorus region and its offshore area as far as 42.5°N. Another warm region along the Romanian Bulgarian coast extending the Bosphorus which was observed in the September 24, 1991 image had disappeared in this image. This may have been caused by a southwesterly wind inducing upwelling as indicated before. The cloud pattern and *in situ* observations of the weather condition during the September, 1991 cruise support this idea.

The structure of the surface temperature field drawn from *in situ* data (OĞUZ *et al.*, 1994) was poorly correlated with the satellite infrared observations, which was not unexpected since these *in situ* data were collected over a one month period. During this interval, atmospheric conditions strongly effected the surface circulation patterns. Thus, the September 1991 satellite images highlight the differences in mesoscale structures between the non-synoptic cruise data

and synoptic satellite data, demonstrating that, at that time, events in the Black Sea were very energetic.

In Figs 5a and 9a, instabilities between warm and fresh (less dense) riverine outflow, and cold open sea water were clearly discerned from the western shelf to the Bulgarian coast. The transport of the cold water in the southwestern Black Sea, which was connected to the cold eddy on the Bulgarian shelf, displays meanders, eddies and filaments as it extends eastwards in a wave pattern as far as Cape Calti. A more pronounced cold region between Cape Kerempe and Cape Bafra may have resulted from the upwelling event which is frequently observed in this region. However, in this case there were more unstable small scale features around the region. The dipole eddy near Arkhangelsky Ridge also persisted on both images. Comparison of the meandering motion along the Anatolian coast on these two successive images show (by following points with fixed phase) an eastward propagation speed of $\approx$ 20 cm.s$^{-1}$ for the meandering motion; a remarkably rapid propagation of wave motions which were superimposed on mean Rim Currents.

One of the more important mechanisms generating these time-dependent motions along frontal regions could be the baroclinic instabilities which developed in the area. Realistic boundary flows with horizontal density gradients are often found to be unstable with small perturbations, and as a result, in many cases the unstable waves grow into large amplitude meanders or paired coherent vortices. Laboratory experiments conducted by CONDIE (1989) showed that the energy of the unstable motions, including coalescent eddies and dipoles, is extracted from the mean flow at the Rossby deformation radius scales, and later transferred to larger scales by nonlinear processes. During the nonlinear growth stage of the instability, it was demonstrated that enhanced meander and eddy growth could occur as a result of relaxation processes, e.g. temporally varying buoyancy forcing, which seems to be more important in the case of retrograde (isobaths and isopycnals slanted in opposite sense) fronts and more effective than the other possible forms of external forcing (such as winds or small topographic variations), (see NIHOUL and JAMART, 1989 for a review). SUR *et al.* (1994) have reviewed CZCS data from 1980 and have found the same region of influence for phytoplankton blooms with similar cross-shelf influences. The meanders and filaments were identified as the main mechanism of exchange between the shelf and open ocean regions, distributing shelf-derived materials into the interior of the basin.

On the image of June 24, 1992, whole region east of Cape Kerempe was covered with cold water which extended to center of the Black Sea. A cold front emanating from the northwestern shelf is apparent, as was seen in the previous month's images. An ongoing wave like meandering motion is also observed between the Bulgarian coast and Cape Kerempe in this image (Fig. 5b).

Nine days later, the large area of cold water to the west of Cape Ince had disappeared but the meandering motion of the cold water although weakened still persisted along the south western coast. The continuation of warm Danube outflow, causing various unstable structures during its advection along the Romanian and Bulgarian shelf regions, was also apparent. A band of cold water at a depth of between 50 m and 2000 m, separating the warm Danube flow along the coast from the warmer offshore water ( $>$ 2000 m) in the western part was seen to be connected to the cold northwestern shelf water (Fig. 7a).

Three days later (Fig. 7b), the temperature gradient decreased throughout the region probably a consequence of wind induced mixing in the upper layer. A more pronounced band of cold water developed along the Romanian, Bulgarian and Turkish coasts and the advection of Danube outflow displayed a warm frontal region between the upwelled water of the shallow western shelf and offshore water. One day later, better developed, small meso-scale features were seen over the entire Black Sea Basin(Fig. 5c). Weakening of the warm Danube outflow and the

mushroom like structure on the Danube Fan are clearly seen in this image. Note also the eddies of various sizes and filamental structures embedded in the meandering motion along the coast especially near Capes Ince, Bafra and Calti.

In Fig. 9b, all of the unstable features which had been observed 20 days earlier (Fig. 7b) had settled down and the warm Danube outflow had disappeared. Remarkable cold regions had developed near the Bulgarian coast (these are frequently observed as a result of wind induced upwelling), and another with various cold filaments occurred near Cape Ince. At this time, there were no cold regions along the Turkish coast as far as Sinop, but within two days (Fig. 9c), another cold feature east of Cape Kerempe started to develop and another large area of cold water developed extending offshore from Cape Ince to Cape Calti.

Analysis of the July 1992 hydrographic data showed a well defined Rim Current following the continental slopes of the Black Sea as the main circulation feature, excluding the region of Batumi gyre (Fig. 5h). Some anticyclonic eddies were also observed along the slope adjoining the NWS. The most striking aspect of the circulation was the coastal attachment of the flow along the Anatolian coast in the southwest region, and its separation later from the coast near Cape Kerempe. In the lee of the separation point a region of upwelling, with important consequences for fish eggs and larvae distribution has been discovered by SUR *et al.* (1994). The data indicated penetration of the surface mixed layer by the upwelled CIW. Figure 5i shows the isolines of surface temperatures. Cold and warm regions in this figure, more or less, correlate with the satellite images of July 1992 (Fig. 9c) although the data are non-synoptic. The near-surface salinity distribution in Fig. 5j shows a frontal region extending around the entire basin

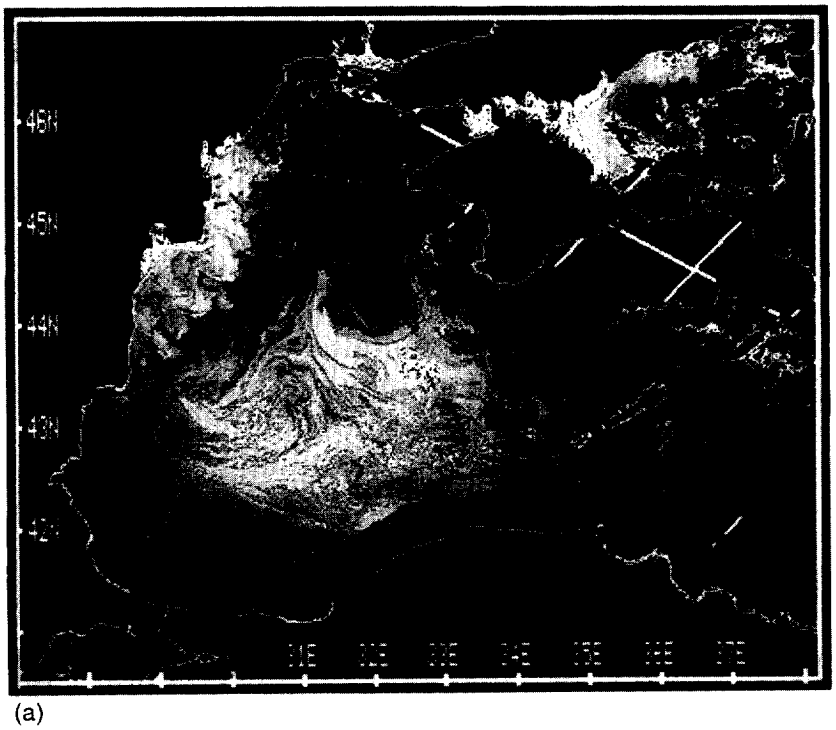


(a)

Fig. 9. Infrared images in 1992; (a) May 22, (b,c) July 26,28.

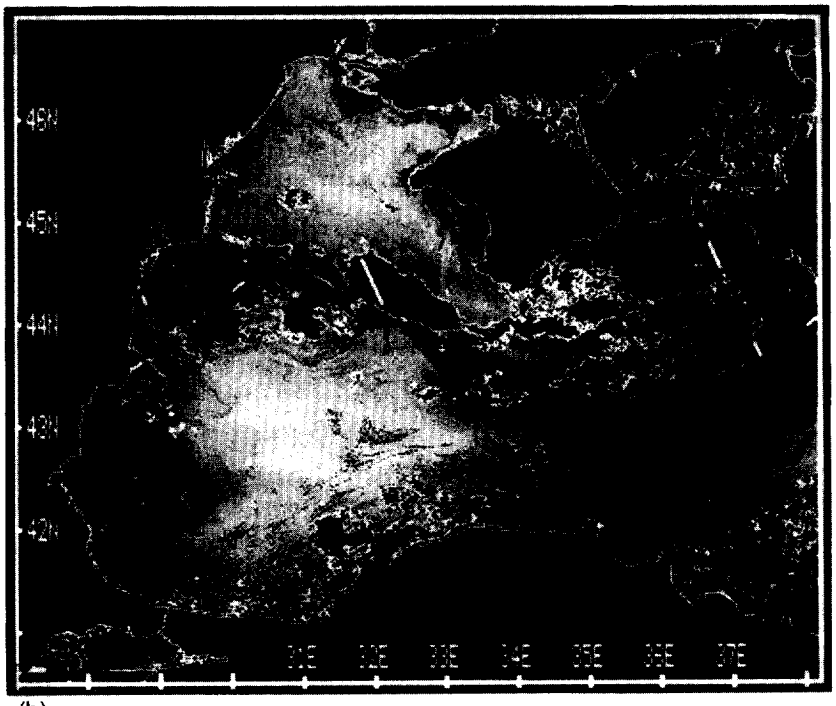


(b)

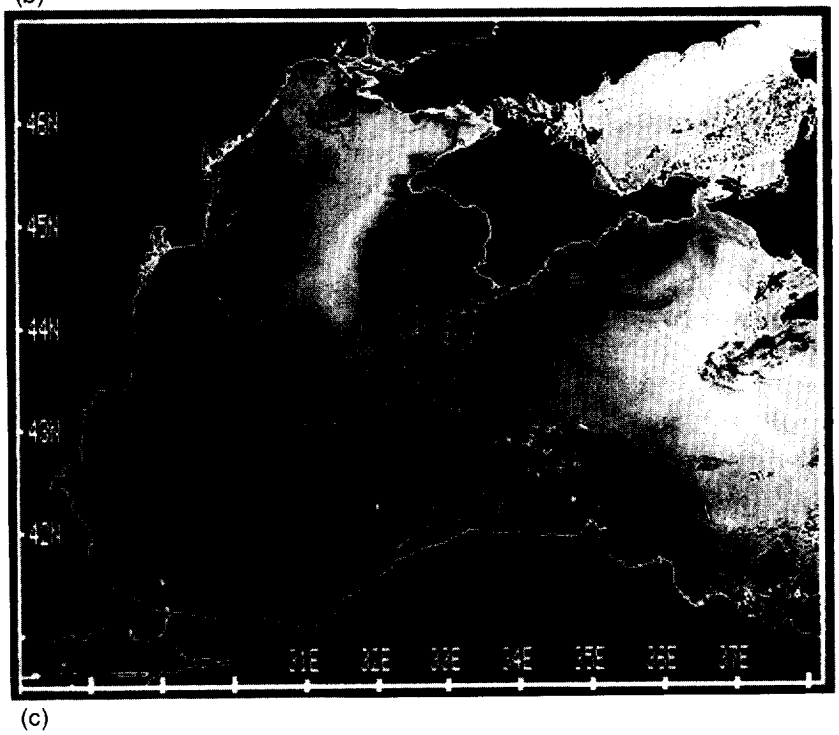


(c)

Fig. 9. Continued

in parallel to the Rim Current with low values of salinity on the coastal side of the front as a result of the southward advection of the Danube water.

Figure 5d shows that in the central basin cold water persisted, as seen in the previous image, and a warm frontal region appeared in the central basin lying from north to south which was also observed in the *in situ* data (Fig. 5i). Development of a cold band of water between Cape Baba and Cape Kerempe is again clearly seen. Note also the filaments connected to Cape Bafra and Cape Calti which have a cyclonic tendency. We believe that these structures are closely correlated to the instabilities which affected the cold nearshore water, observed at the end of the previous month. Another long filament ( $\approx$ 250 km), containing cold water originating from NWS, was located off Burgaz Bay. Just one day later (Fig. 5e), temperature gradients had decreased throughout the whole basin although the all hydrographic features seen on the previous image were still in evidence. Note also the small scale filamental structure emerging from the upwelling region near Cape Kerempe.

Eight days later (Fig. 5f) nearly all the cold upwelled water had disappeared from the upwelling region along the Anatolian coast, but another region of cold water had developed east of Cape Ince with various offshore filaments along the coast. Note that this area was also partially covered by cold water on the image of August 2, 1992 (Fig. 5d). Other striking features are the warm filamental fronts off the Romanian coast along the plume of the Danube outflow. Two days later, this plume was more pronounced (Fig. 7c) and was covering the western shelf with various offshore eddies and squirts. Another structure repeatedly seen is the cold water between Cape Baba and Cape Kerempe. The Rim Current along the Anatolian coast advected the cold water west of Cape Ince towards the east which is supported by the filaments originating from Cape Kerempe and Cape Ince with their eastward tendencies. At the beginning of September 1992, an enhanced structure of upwelled water was observed around Cape Kerempe (Fig. 7e). Filaments extended 90 km offshore and covered all the region between Filyos River and Cape Ince except for the area to the east of Cape Kerempe.

## 5. SURFACE LAYER CURRENTS AND MESOSCALE THERMAL PATTERNS IN APRIL 1993

One of the fundamental questions asked in satellite oceanography is how closely does the temperature distribution at the surface reflect the upper layer circulation pattern for the mid-scale spatial variabilities. Hydrographic studies of this problem require detailed quasi-synchronous current and temperature measurements in a specific region. Such data can be obtained by means of satellite infrared records, accompanied by *in situ* ADCP current ship-born measurements. One such successful experiment addressing this question in the Algerian Current region is discussed by ARNONE *et al.* (1990).

In April 1993, both CTD (conductivity, temperature, depth) and ADCP measurements were carried out in the Black Sea, when a very turbulent flow pattern with embedded coherent features was observed. The sea surface dynamic topography calculated from hydrographic and ADCP current data (GÜNGÖR, 1994) for this period only showed up the coarse meso-scale and synoptic features, including the boundary current and a series of anticyclonic eddies to the west of the Crimean Peninsula and extending along the western continental shelf, around the periphery of the cyclonic central region (Fig. 10a). The ADCP horizontal current vectors at 10 m (Fig. 10b) coincided with these features and verified the presence of a swift meandering boundary current with a speed of up to 100 $cm.s^{-1}$ along the continental slope region, and various relatively weaker flows in the north-western shelf and in the central parts of the sea (5-15 $cm.s^{-1}$). More

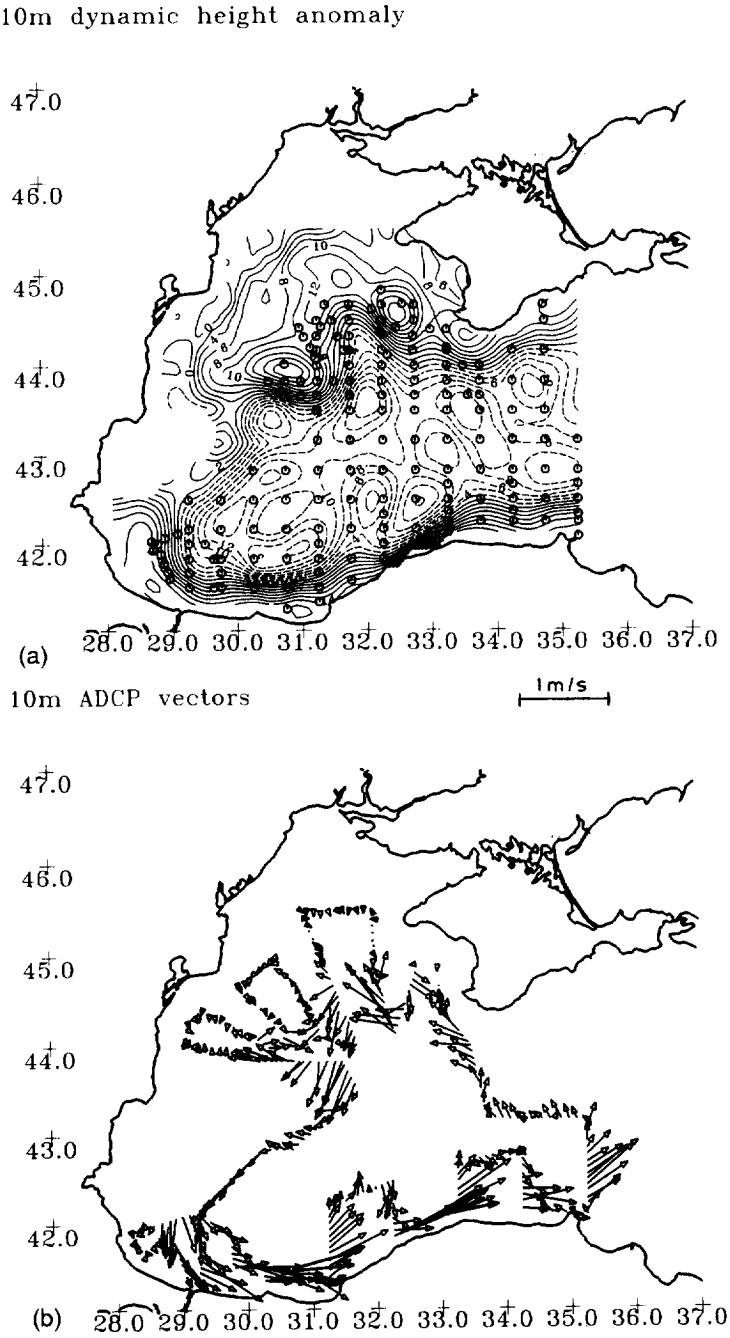


Fig. 10. (a) Dynamical topography map, (b) ADCP current measurements (1 cm corresponds to 50 cm.s − 1 speed); at 10 m depth, and (c,d) Surface temperature and salinity maps of the CoMSBlack-93 cruise.

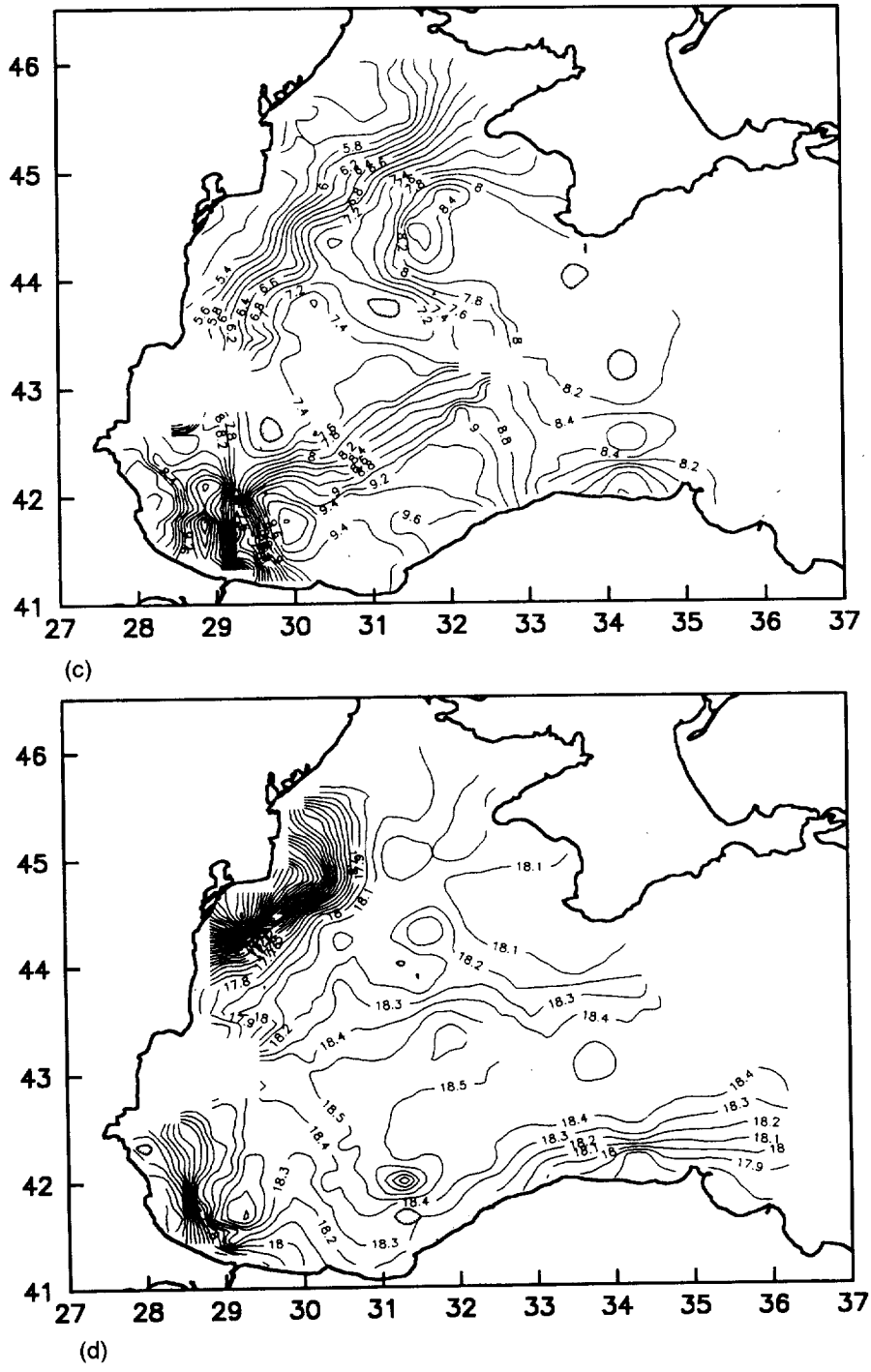


Fig. 10. Continued

detailed ADCP track data revealed the complex mesoscale current structures better, so preferably the high resolution satellite thermal images be compared with these data, especially in the zones of high spatial variability (Rim Current meanders and eddy fronts).

Comparison of current vector distributions at 10 m and 20 m levels presented in OĞUZ *et al.* (1996) shows almost identical structures allowing us to infer the vertical homogeneity of the upper layer circulation, so the ADCP data are a good basis for the interpretation of sea surface satellite imagery. The nearest cloud free AVHRR scene to the cruise data obtained on April 19, 1993 (Fig. 11a) shows a meandering band of warm water which corresponds to the Rim Current west of Sevastopol. To the south, along 44.2°N the cold water area apparently forms a flow divergence separating into two branches. The amplitude of the cold anomaly is – 1.2°C at the base of the northern current branch of cyclonic meander west of the Crimea. To the west of this meander, the anticyclonic Sevastopol eddy, with a diameter of 55 km, is centered at 44.5°N, 32.1°E. Further to the southwest there is another cyclonic meander separating the Sevastopol eddy from the next cold anticyclone centered at 44.2°N, 30.5°E. Another onshore bifurcation (anticyclonic) generated the Kaliakra Eddy (centered at 43.3°N, 29.8°E) which had shifted towards the south-west relative to its position the previous summer (Table 1).

Also in Fig. 11a, NWS is colder (1.5–2.0°C) than the region along the continental slope (Fig. 10c) as a result of convective cooling during the preceding winter. Near the western coast, the Danube waters are well defined, being warmer (by about 1.5°C) than the surrounding shelf water. Plumes discharging from the three delta tributaries of the Danube (Kilija, Sulina and St George) are clearly distinguished; these then merge into a narrow band of warm water which flows along the coast to form the warm anticyclonic eddy south of Cape St. George. Between the near-shore jet and the Rim Current flowing along the shelf edge is a cold zone of shelf water connected to north-eastern shelf. This meandering band of cold water forms a sharp cold frontal structure towards offshore wherever it meets the Bosphorus Canyon. It is also clearly seen on the temperature and salinity isolines of hydrographic data which show a colder and more saline water front on the offshore side of the Bosphorus lying perpendicularly to the coast (Fig. 10c,d). This is also verified by the vertical hydrographic transect at that section (not shown). Warmer water in the southwestern sector along the Anatolia region already shows some heat gain from the atmosphere as the heating season had begun. The annual mean heat flux changes sign at about 43°N, so that the southern basin gains heat from the atmosphere whereas the northern sector continued to loose heat to the atmosphere (OĞUZ *et al.*, 1995). A cold region extending all the coast from Filyos River up to Cape Ince is also seen in this same image.

Along the southern sea shore, The Rim Current jet is distinguished by its high temperature. To the north of this jet, an anticyclonic eddy, possibly generated by a Rim Current instability, was located offshore of the Bartin River (centered at 42.5°N, 31.7°E) attracts attention. This structure captures cold water from offshore and traps it within an anticyclonic filament with a diameter of $\approx$ 40 km and temperature gradient of $\approx$ 6°C between the center and periphery. Note that evidence of this small eddy is also revealed in the ADCP measurements (Fig. 10a,b).

Four days later (Fig. 11b), the meandering motion of the warm water originating from the southwestern sector had become more pronounced and was following the Anatolian coast up to Arkhangelsky Ridge. The filamental structure with the anticyclonic tendency off the Bartin River retained its position and strength during this 4 day period. Another interesting feature is that the cold water seen originating from the west of Cape Kerempe, where upwelling frequently occurs; it was observed on the previous image, following the meandering warm water mentioned above as a cold band of water on its inshore side. Whenever this cold band of water reaches

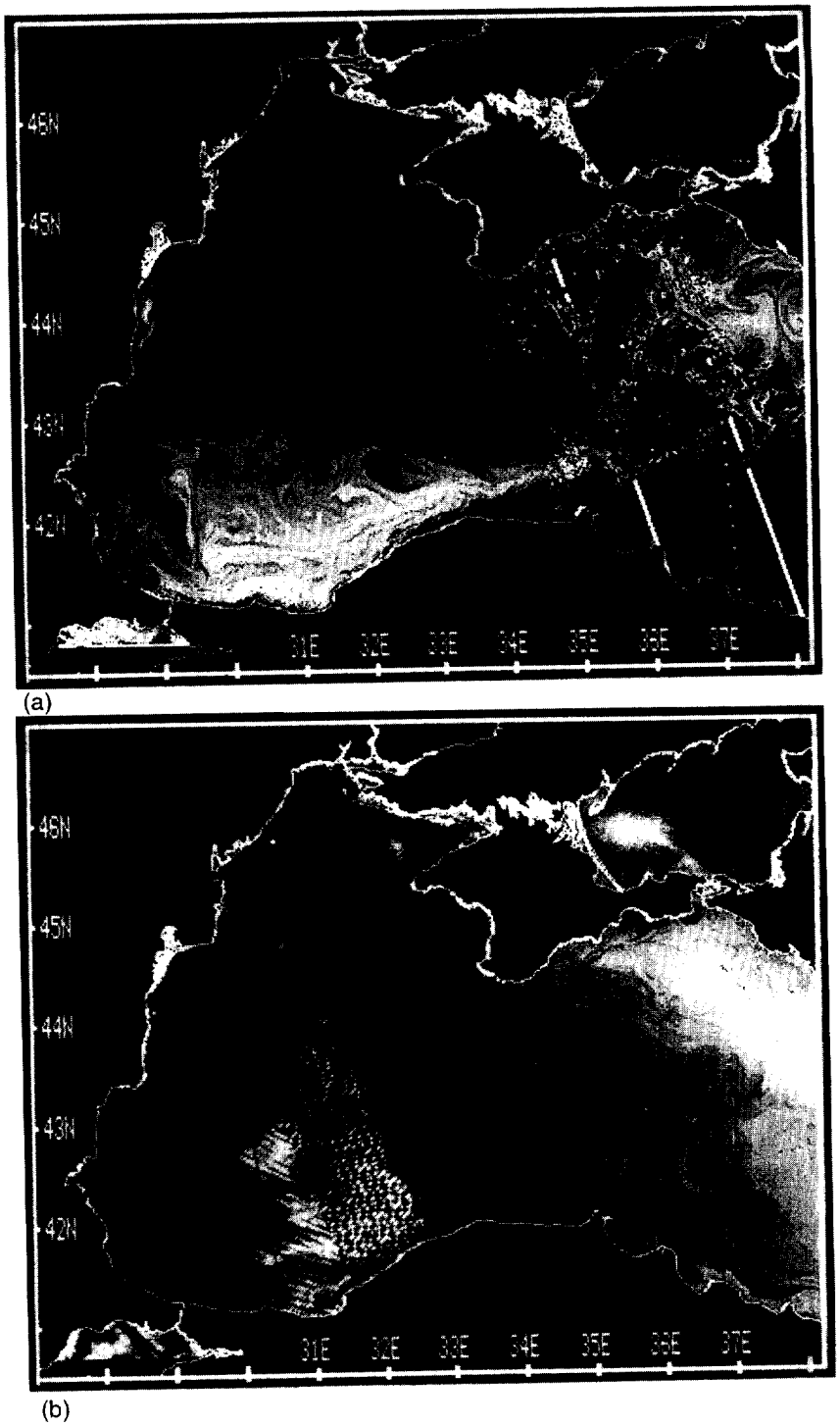


Fig. 11. Infrared images in (a–c) April 19, 23 and 27, 1993.

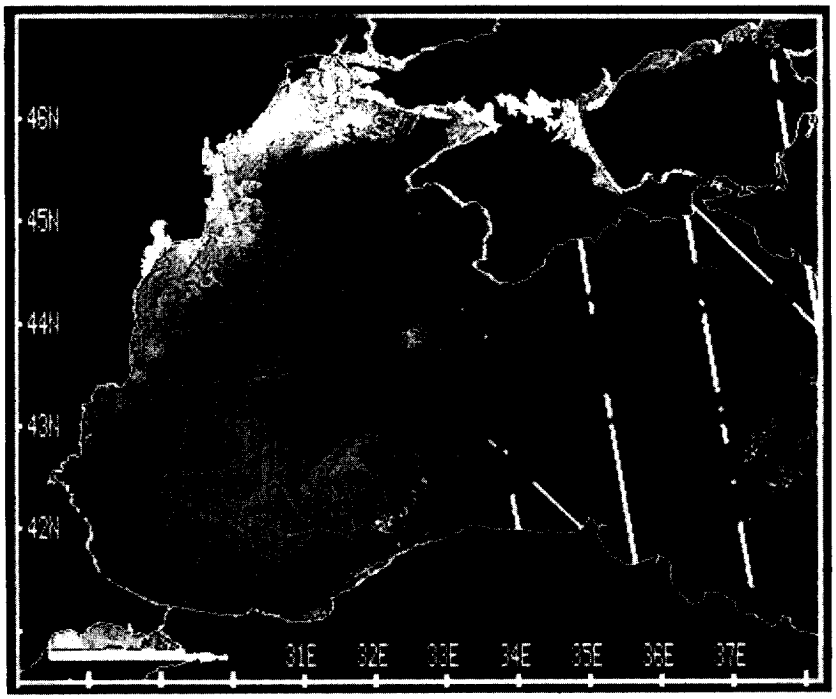


(c)

Fig. 11. Continued

the Arkhangelsky Ridge, it is deformed and forms a mushroom-like structure aligned with the ridge, with the remaining part of this flow continuing eastwards along the coast.

In the image of April 27, 1993 (Fig. 11c), a fully developed turbulent structure of the Boundary Current can be seen along the western shelf. As indicated in the May '92 images, small scale features resulting from frontal instabilities occurred along the shallow southwestern shelf. The warm outflows of the Dnestr and Danube Rivers, and the cold patch of water on the northwestern shelf can be seen. The cold northwestern shelf water becomes entrained between the warm nearshore and continental slope waters as it proceeds south along the coast. The meandering structure of the cold water connected to the northern sector was more developed and extended along the southwest coast showing a wave like structure with a wavelength of $\approx$ 140 km. In the deep region (2000 m) of the western Black Sea, warm water preserved its identity, and the core of the cold feature off the Bartin River also kept its position, although it had been eroded by the surrounding warm water.

The April 27, 1993 image shows substantial changes from previous scenarios, as a result of fast adjustments to the surface circulation because of external (intensive sun heating, wind weakening) and internal (CIW evolution, riverine water transformation) forcing. In particular, the Sevastopol eddy appears to have stretched in a meridional direction and enlarged to 70 km. The cyclonic meander to the west of it also intensified. The second anticyclone, located along the meander, has moved further south (centered at 43.9°N, 30.6°E) and decreased in size. The intensive eddy generation off the Danube deltas and to the south of them are yielding clearly visible horizontal mixing patterns of the shelf and river waters, predominantly involving cyclonic

eddies with diameters of 12–18 km (maximum dimensions 18–22 km). The Boundary Current can not be yet observed as a continuous jet in the south-western region but instead, a system of 5–6 interacting eddies are developed which are thus transferring water to the east. Such reformation of the flow is a characteristic of the spring-summer season in the Black Sea (STANEV *et al.*, 1988; EREMEEV *et al.*, 1991).

The distributions of ADCP current vector and satellite images together (Figs 10 and 11), show almost total correspondence of flows measured *in situ* and thermal structures at the sea surface along the ship's track for April 19, 1993. The velocity maxima coincide with the locations of temperature gradient of the Rim Current and the vector directions correspond to satellite derived flow configuration. Moreover, the satellite data assist us in the interpretation of ADCP current data by explaining several peculiarities in vector distribution as a manifestation of mesoscale dynamic features. Examples are: (i) The Rim Current thermal pattern west of Crimea and alternating meanders and eddies allow us to fill the gaps of ADCP measurements between the ship tracks; (ii) The northward directed vector observed in the middle of the ships track along 42.4°N between 31.3 and 32.3°E, and also the south-westward currents in the northern sector of the next meridional track can only be understood in the context of the satellite data showing how the ship track had passed through the south-western periphery of the anticyclonic eddy discussed above; (iii) To the north of the Bosphorus, at 42.0–42.2°N, convergence of the vectors is observed. From the satellite image it could be inferred that this phenomenon was the confluence of two flows: one a warm jet coming from the north along 29.4°E, the other a cold tongue of water coming from the north-west on the shelf side.

Noted that, the close correlation between measured current parameters and thermal circulation structures in this case has obvious seasonal characteristics, since during the cruise the conditions observed were typical of those preceding development of the seasonal thermocline. Later reformation of the temperature field occurred thus yielding the differences between the images in Fig. 11a,c. It remains uncertain whether these changes reflect a close relation between peculiarities in the mesoscale temperature and current fields during the summer months. This question requires further experimental investigations.

## 6. CONCLUSIONS

Joint analysis of satellite and ship data confirmed that coherent eddies and turbulent features are quite common in the black sea. Often the coherent structures emerge, decay, or change form and position with fascinating rapidity. Diverse manifestations on the sea surface and intensive interaction between sub-basin and small-scale features makes the problem of their investigation considerable because both the coherent anticyclonic eddies and large amplitude meanders of the coherent jet flow along the basin periphery, display rapid evolution and develop significant transport around the basin and exchanges between the coastal and open sea.

During the summer season, peculiarities in the anticyclonic eddies on the right hand side of the Rim Current are related to the volume of CIW in these anticyclones. If the thickness of CIW in the eddy center exceeds peripheral values (i.e., thermocline is closer to the sea surface), the turbulent entrainment mechanism leads to the appearance of a cold anomaly at the center of the anticyclonic eddy. On the other hand, when the volume of CIW inside the anticyclone decreases, interfacial elevation gets smaller in the center, then a warm anomaly is expected to develop in the eddy's center after summer.

The September 1991 satellite images displayed a weak correlation between the non-synoptic

cruise data and synoptic satellite data for the mesoscale structures, supporting the hypothesis that events in the Black Sea are very energetic. Remarkable cold anticyclones occurred off the Kerch Strait in 1991 and 1992, but satellite images obtained during the summer of 1992 demonstrated different mesoscale dynamic patterns than seen the previous summer; especially with the well-defined short wave structure in 1991, and both short and long wave features in 1992 together with the meandering Rim Current jet in this region.

The satellite images of May 1992 display how the mass of warm water emanating from the Dnestr and Danube Rivers was developing instabilities along the front at the shelf break which were progressing westwards in the spring. This is expected during March and May as a result of peak values of the Danube out flow (e.g., SUR *et al.*, 1994). Small-meso scale features, such as filaments, dipole eddies were present over the entire sea but especially so in the western region.

An overview of satellite data also indicate there were repeated upwelling events with rapidly varying distribution along the Turkish coast between Cape Baba and Cape Ince during the spring and summer months. Although the basic mechanisms leading to these upwellings remain largely unexplained, it is suggested that the interaction of the currents with the coastline geometry and bottom topography (SUR *et al.*, 1994), as well as surface divergences within the shallow mixed layer overtopping CIW could induce upwelling without the need for wind forcing. These kind of transient upwelling events along fronts and unstable current systems are known to exist in other regions (e.g. MILLOT, 1991).

The ADCP current vectors and thermal structures at the sea surface displayed very good correlation on April 19, 1993. The velocity maxima coincided with the locations of high temperature gradient associated with the Rim Current and the vector directions corresponded to the satellite derived flow configuration. It should also be noted that; the close correlation between measured current vectors and thermal structures in the case considered has obvious seasonal characteristics since during the cruise conditions were typical of those preceding development of the seasonal thermocline.

Later it is seen that the Rim Current which flows along the continental slope, is spread along the coast and across the frontal region by turbulent motions, which either result from instability mechanisms or are initiated by interactions with sudden variations in along-shore topography. Transport by the Rim Current along the basin periphery and the cross-shelf transports created along this current are important for the spreading of productivity and the subsequent basin-scale processes, and sets the time and space scales of a succession of plankton blooms and their transformation into higher trophic levels. It is also recognized that these circulation features are important for the migration/spawning behavior of the pelagic fish stocks of the Black Sea.

## 7. ACKNOWLEDGEMENTS

This study was made possible through the TU-FISHERIES, the TU-BLACK SEA Projects of the NATO Science for Stability Program, and a NATO Linkage Grant between the IMS-METU Erdemli, and MHI Sevastopol; and was partially supported by the Turkish Scientific and Technical Research Council (TÜBITAK).

## 8. REFERENCES

ARNONE R. A., WIESENBURG D. A. and SAUNDERS K. D. (1990) The origin and characteristics of the Algerian Current . *Journal of Geophysical Research, 95* **C2**, 1587–1598.

BLATOV A. S., BULGAKOV N. P., IVANOV V. A., KOSAREV A. N. and TUZHILKIN V. S. (1984) Variability of Hydrophysical Fields of the Black Sea., Hydrometeoizdat, Leningrad, 240pp. (in Russian).

CONDIE S. A. (1989) Mesoscale structures on density driven rim currents, In: *Mesoscale/Synoptic Coherent Structures in Geophysical Turbulence*, J. C. J. Nihoul and B. M. Jamart, editors, Elsevier, Amsterdam, 197–210.

EREMEEV V. N., IVANOV V. A. and TUZHILKIN V. S. (1991) *Climatic manifestations of the intra-year variability of the Black Sea shelf zone hydrophysical fields*. Marine Hydrophysical Institute Pre-print, Sevastopol, 52pp. (in Russian).

FEDOROV K. N. and GINSBURG A. I. (1988) *Surface layer of the Ocean*. Hydrometeoizdat, Leningrad, 304pp. (in Russian).

FEDOROV K. N. and GINSBURG A. I. (1989) Mushroom-like currents (Vortex Dipoles); One of the most widespread forms of non-stationary coherent motions in the ocean. In: *Mesoscale Synoptic Coherent Structures in Geophysical Turbulence*. J. C. J. Nihoul and B. M. Jamart, editors, Elsevier, Amsterdam, 1–14.

GRISHIN G. A., ILYIN YU. P., KIKHAY YU. V., KUNITSA V. E., MAKEEV I. G. and KHOROLICH N. G. (1989a) Analysis of the eddy-like temperature disturbance evolution in the Black Sea in July, 1987 (Based on the NOAA Satellite Data). In: *Transactions of 5th Satellite Hydropysics Seminar, Sevastopol*. Deposed in VINITI, No 3765-B89, 166–191 (in Russian).

GRISHIN G. A., ILYIN YU. P., KALININ E. I. and KIKHAY YU. V. (1989b) Surface manifestations of the main Black Sea Current structure by satellite and in-situ data. In: *Transactions of 6th Satellite Hydropysics Seminar, Sevastopol*. Deposed in VINITI, No 6176-B89, 233–244 (in Russian).

GÜNGÖR H. (1994) *Multivariate objective analyses of ADCP and CTD measurements applied to the circulation of the Laventine Sea and Black Sea*. M. S. Thesis, Institute of Marine Sciences, Middle East Technical University.

HANEY R. L. (1971) Surface thermal boundary condition for ocean circulation models. *Journal of Physical Oceanography* **1**, 241–248.

ILYIN YU. P. (1989) Jet flow diametrical circulation effect on the day-time heating thermal featuresformation (in application to infrared images analysis). In: *Transactions of 6th Satellite Hydropysics Seminar, Sevastopol*. Deposed in VINITI, No 6176-B89, 245–252 (in Russian).

ILYIN YU. P. and GRISHIN G. A. (1992) Quantitative analysis of the surface currents by satellite imagery: Inverse problem for tracer transfer model. *Investigations of Earth from Space* **5**, 65–71.

IVANOV L. I. (1992) Cold Intermediate Water formation in the western Black Sea as derived from 1992 data. In: *Problems of the Black Sea*. Sevastopol, 78–89.

IVANOV V. A. and ILYIN YU. P. (1993) Estimation of fluctuation parameters for the sea surface temperature obtained along the southern seashore of the Crimea Basin on spaceborn Data. *Investigations of Earth from Space* **2**, 11–18.

KRAUS E. B, BLECK R. and HANSON H. P. (1988) The inclusion of a surface mixed layer in a large-scale circulation model. In: *Small-scale turbulance and mixing in the ocean*. J. C. J. Nihoul and B. M. Jamart, editors. Elsevier, Amsterdam, 51–62.

LATUN V. S. (1990) Energy supply of the Black Sea deep anticyclonic *eddies. In: Complex Oceanographical Investigations of the Black Sea*. V. N. Eremeev, editor, Sevastopol, 10–12 (in Russian).

LINDEN P. F. (1991) Dynamics of fronts and eddies. In: *Proceedings of the international school of Physics, Enrico Fermi, Course CIX, Nonlinear Topics in Ocean Physics*. A. R. Osborne, editor. North-Holland, Amsterdam, 313, 351.

MILLOT C. (1991) Mesoscale and seasonal variabilities of the circulation in the western Mediterranean. *Dynamics of Atmosphere and Oceans* **15**, 179–214.

NIILER P. P. and KRAUS E. B. (1977) One-dimensional models of the upper ocean. In: *Modelling and Prediction of the upper layer of the Ocean*. E. B. Kraus, editor, Pergamon Press, 143–172.

NIHOUL J. C. J. and JAMART B. M. (1989) *Mesoscale Synoptic Coherent Structures in Geophysical Turbulence*. Elsevier, Amsterdam.

OĞUZ T., LATUN V. S., LATIF M. A., VLADIMIROV V. V., SUR H.İ, MARKOV A. A., ÖZSOY E., KOTOVSHCHIKOV B. B., EREMEEV V. V. and ÜNLÜATA Ü. (1993) Circulation in the surface and intermediate layers of the Black Sea. *Deep-Sea Research* **40 (8)**, 1597–1612.

OĞUZ T., AUBREY D. G., LATUN V. S., DEMIROV E., KOVESHNIKOV L., SUR H. İ., DIACONU V., BESIKTEPE S., DUMAN M., LIMEBURNER R. and EREMEEV V. (1994) Mesoscale circulation and thermohaline structure of the Black Sea observed during HydroBlack 1991. *Deep-Sea Research*, **8**, 603–628.

OĞUZ T., AUBREY D. G., BESIKTEPE S., IVANOV L. I., DIACANU V. and ÜNLÜATA Ü. ADCP observations of the Western Black Sea Rim Current. *Deep-Sea Research II* 1996 (in press).

OĞUZ T., RIZZOLI P. M. and AUBREY D. G. (1995) Wind and thermohaline circulation of the Black Sea driven by yearly mean climatological forcing. *Journal of Geophysical Research*, **100**. *No.* **C4**, 6845–6863.

ROBINSON I. S. (1991) *Satellite Oceanography. An Introduction for Oceanographers and Remote-Sensing Scientists*, Ellis Horwood, 455pp.

STANEV E. V. TRUHCHEV D. I. and ROUSSENOV V. M., (1988) *The Black Sea Water Circulation and Numerical Modeling of Currents*. Sofia, 222pp.

SUR H. I., ÖZSOY E. and ÜNLÜATA Ü. (1994) Boundary current instabilities, upwelling, shelf mixing and euthrophication processes in the Black Sea. *Progress in Oceanography* **33**, 249–302.

SUR H. I., ÖZSOY E., ILYIN Y. P. and ÜNLÜATA Ü. (1996) Coastal/deep ocean interactions in the Black Sea and their ecological/environmental impacts. *Journal of Marine Systems* **7**, 293–320.

ÜNLÜATA Ü., AUBREY D. G., BELBEROV Z., BOLOGA A., EREMEEV V. and VINOGRADOV M. (1993). International program investigates the Black Sea. *EOS*, **36**, 408–412.